Chapter 4

Synthesis and mesomorphic properties of

Part I

(i) 1, 3-Phenylene bis [4-(4-*n*-alkyloxycarbonylphenyliminomethyl)benzoates]

Part II

(ii) 1, 3-phenylene bis [4-(4-*n*-alkyloxycarbonylbenzylideneamino)benzoates]

Introduction

A smectic phase with chiral C_1 symmetry (triclinic symmetry), which is the lowest possible symmetry, was predicted by de Gennes [1]. This phase is referred to as SmC_G where G stands for general. However, no experimental evidence could be found for this mesophase in calamitics up to date. In 1998, Brand *et al*. [2] gave a theoretical model for the existence of this mesophase in a bent-shaped compound. In SmC_G phase, the molecules have an orientation where all the three principal axes make an angle with the smectic layers different from 0˚ and 90˚. This results in a double tilted structure, which involves the tilt of the molecular plane with respect to the layer normal (clinicity), and the tilt of the molecular long axis (director) with respect to the layer normal (leaning) along the molecular plane as shown in figure **4.1**. Thus, the director tilt is described by two angles, tilt angle θ and the leaning angle ϕ. This gives rise to syn leaning and anti leaning structures in addition to synclinic and anticlinic structures found in the B_2 phase. The layer polarization has both in-layer and out-of-layer components and may form both ferro and/or antiferroelectric phases. Considering these facts, eight different possible sub-phases have been

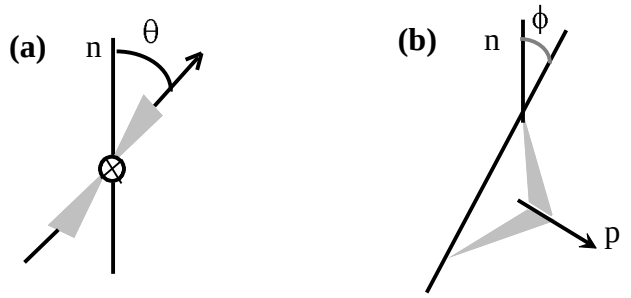

Figure 4.1: A graphical representation of the tilt of the bent-core molecules in the SmC_G phase. (a) Tilt of the molecular plane with respect to the layer normal; (b) leaning of the molecular long axis with respect to the layer normal in the tilt plane. θ-tilt angle, ϕ- leaning angle, n-layer normal, p-polar direction.

predicted by the association of two layers of different forms of SmC_G [2]. There are a few reports of experimental realization of this mesophase in bent-core compounds but an unambiguous evidence for this structure is not available so far [3-7].

Although a few thousand bent-core compounds have been synthesized and their mesomorphic properties investigated, a proper understanding of the structure-property relationships is still elusive. Amongst all the mesophases exhibited by BC compounds, the SmCP (B_2) phases (two homochiral-SmC_sP_F, SmC_aP_A and two racemic- SmC_aP_F, SmC_sP_A structures) are not only frequently encountered but are also investigated most extensively. Among all the different types of liquid crystals, perhaps the B_7 phase exhibits the most beautiful and fascinating textures. The B_7 phase was first observed [8] in a Schiff's base BC compound derived from 2-nitroresorcinol. This fascinating phase was subsequently observed in a number of compounds obtained from 2-cyanoresorcinol [9-12]. The B_7 phase occurring in this type of compounds and investigated so far do not switch electro-optically at least up to about 40 $V\mu m^{-1}$ except for two antiferroelectric B_7 sub-phases [12].

Remarkably, there are a number of compounds, which do not contain strongly polar substituents but the mesophases exhibit the beautiful optical textures shown by the B_7 phase. These mesophases have also been designated as B_7 despite the fact that their XRD pattern is different from that of the standard B_7 material [8]. These mesophases respond to an applied electric field and both ferroelectric [4, 13, 14] and antiferroelectric [5, 15, 16] structures have been found. At the present time two different structural models for this switchable B_7 phase have been proposed. One model [3] corresponds to a SmC_G structure with a triclinic symmetry where an out-of-layer polarization component is assumed. The other model [17] suggests a polarization modulated, layer undulated structure stabilized by polarization splay for the ferroelectric mesophase as exhibited by MHOBOW [14] (the structure of MHOBOW is shown in Chapter 5). It should be pointed out that in such a structure both in-layer and out-of-layer polarization components are possibly present at least at the defect areas. In order to overcome the discrepancy with regard to the nomenclature, it has been suggested recently [18] to assign the symbol B_7' for these mesophases.

In this chapter, the synthesis and mesomorphic properties of two novel homologous series (series **4.A** and **4.B**) of five-ring bent-core compounds derived from resorcinol have been described. These are symmetrical Schiff's base esters and contain two terminal *n*-alkyl carboxylate groups. These two series of compounds have the same molecular structure but differ only in the orientation of the azomethine linking group.

Part I

In this part, the synthesis and mesomorphic properties of compounds of series **4.A** are discussed. These compounds have the general molecular structure shown below (structure **4.1**).

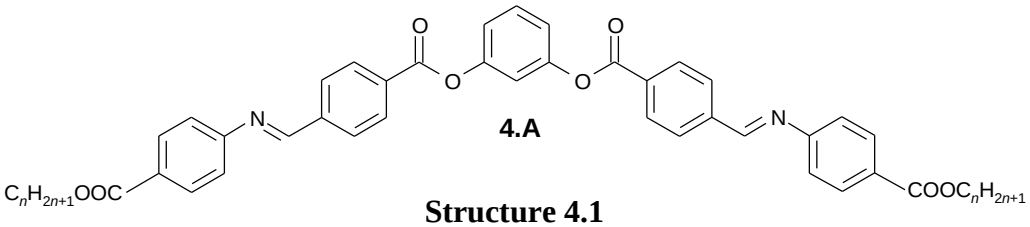

Structure 4.1

Synthesis

The symmetrical five-ring bent-core compounds were prepared following a synthetic pathway shown in scheme **4.1**. 4-Nitrobenzoic acid and 4-formylbenzoic acid were obtained commercially and used without further purification. Commercially obtained resorcinol was purified by column chromatography followed by crystallization. 4-Nitrobenzoic acid, **4.a** was esterified with an appropriate aliphatic alcohol, **4.i** using *N*, *N*′-dicyclohexylcarbodiimide (DCC) and 4-(*N*, *N*-dimethylamino)pyridine (DMAP). Then, the nitro group of ester **4.b** was reduced using 5% Pd-C catalyst in an atmosphere of hydrogen to yield the amine ester **4.c**. This was reacted with 4-formylbenzoic acid, **4.ii** in refluxing toluene in presence of a trace of acetic acid to furnish compound **4.d**. In the final step two equivalents of compound **4.d** was treated with 1,3-dihydroxybenzene, **4.iii** in presence of DCC and DMAP in dry dichloromethane which provided the required mesogenic materials **4.A**. All the compounds were purified by column chromatography followed by repeated crystallization using suitable analytical grade solvents.

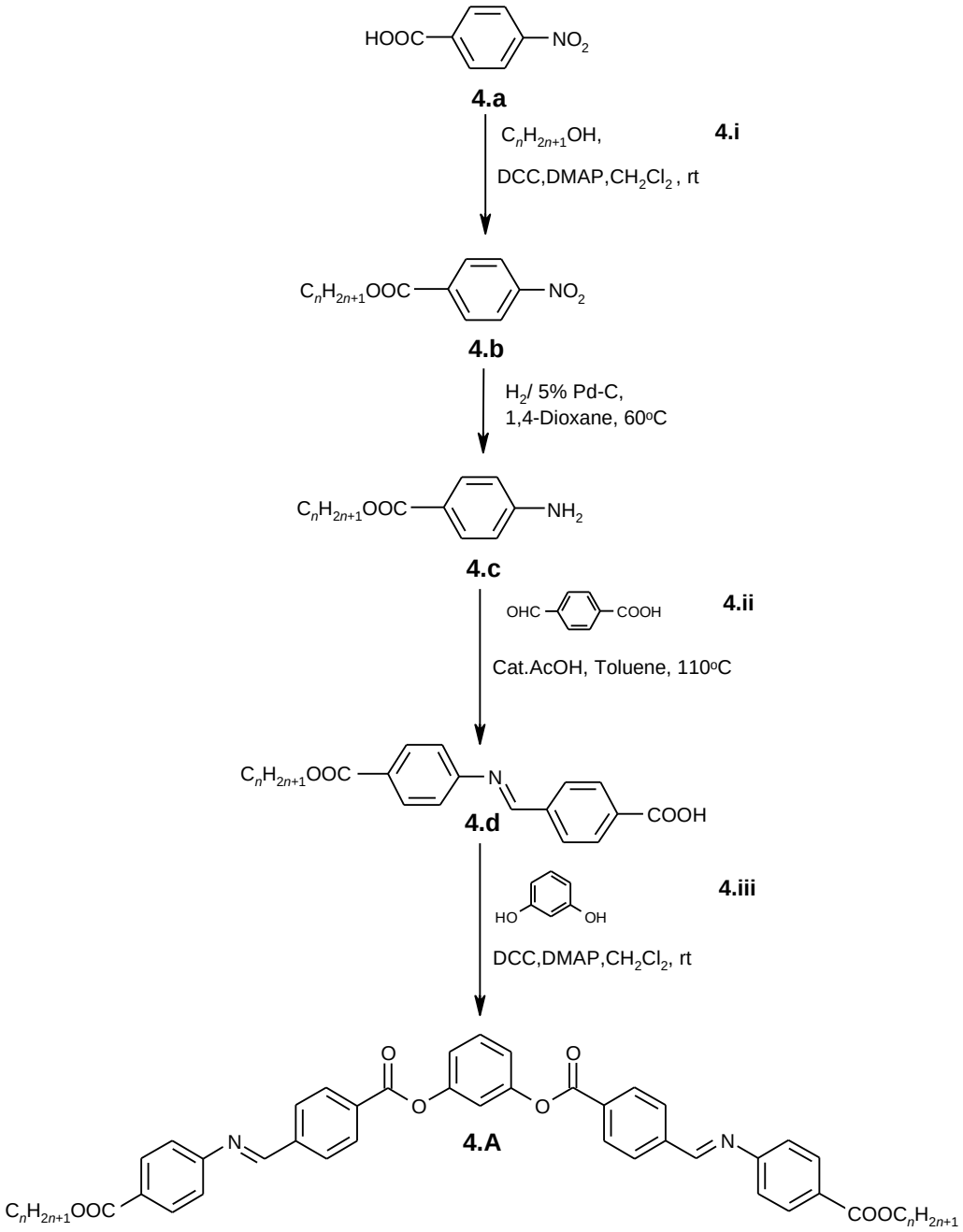

Scheme 4.1: Synthetic scheme followed for the preparation of bent-core compounds, 4.A.

Results and Discussion

All the compounds investigated are liquid crystalline except compound **4.A.1**. The transition temperatures and the associated enthalpy values for these compounds are summarized in table **4.1**. Compounds **4.A.2-6** exhibit the same type of mesophase, which are all enantiotropic. When a sample of compound **4.A.2**, sandwiched between a glass slide and a coverslip was cooled from its isotropic state and observed under a polarizing microscope, a fan-shaped texture was seen as shown in figure **4.2a**. When the inner surfaces of the substrates were treated for homeotropic alignment, a schlieren texture was obtained (figure **4.2b**) indicating a tilt of the optic axis with respect to the layer normal. This was confirmed by X-ray studies, which is described later. Compounds **4.A.3** and **4.A.4** also exhibit similar textural behaviour. In contrast however, when samples of compounds **4.A.5** and **4.A.6** are cooled slowly from the isotropic state, lath-like textures develop with stripes running across them (figure **4.2c** and **4.2d**) and these are independent of temperature. This suggests the existence of a multidomain structure with synclinic tilt of the molecules in each domain and alternating molecular tilt directions from one domain to the next as reported earlier [19]. Stripes are indicative of domain boundaries where the tilt direction changes. In fact similar patterns have been seen for the B_2 phase exhibited by compounds derived from 1-substituted naphthalene 2, 7-diol [20] as well as 4-bromo- or 4-chloro-resorcinol [21]. On the basis of these observations the mesophase exhibited by compounds **4.A.2-6** has been identified as B_2 (SmCP) phase. Their antiferroelectric or ferroelectric, and anticlinic or synclinic structures will be discussed later, on the basis of other experimental investigations.

Although, compounds **4.A.7-9** display one mesophase on heating the crystals, transition to a metastable state was clearly seen both under a polarizing microscope and on a DSC thermogram. A typical DSC thermogram obtained for compound **4.A.8** is shown in figure **4.3**. The accompanying enthalpy is very small indicating a 2^{nd} order transition.

The higher temperature phase exhibits textures consisting of helices, myelin-like pattern etc. that are normally seen for a B_7 phase, when the respective isotropic liquids are cooled very slowly. Such beautiful patterns obtained on slow cooling of the isotropic liquid of compound **4.A.7** are shown in figure **4.4**.

Table 4.1: Transition temperatures (˚C) and the associated enthalpy values (kJ mol^{-1}, in italics) obtained for the compounds of series 4.A.

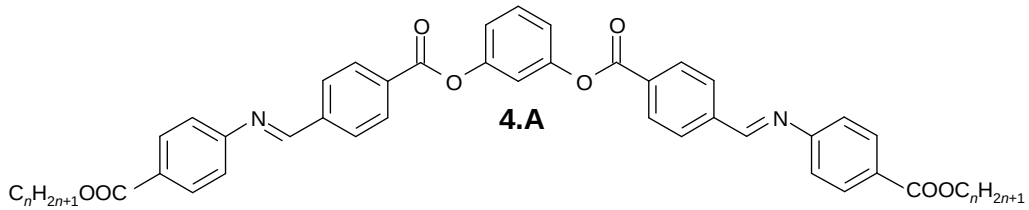

4.A

Compound	*n*	Cr		B_2'		B_7'		B_2		I
4.A.1	6	.	142.0	-		-		-		.
			84.5							
4.A.2	7	.	140.5	-		-		.	141.5	.
			65.0						*18.0*	
4.A.3	8	.	140.0	-		-		.	142.5	.
			58.5						*20.5*	
4.A.4	9	.	132.5	-		-		.	143.0	.
			60.0						*18.0*	
4.A.5	10	.	134.5	-		-		.	142.5	.
			66.5						*18.5*	
4.A.6	11	.	132.5	-		-		.	142.5	.
			64.0						*20.5*	
4.A.7	12	.	133.0	(.	128.5)	.	140.5	-		.
			70.5		*0.07*		*19.0*			
4.A.8	13	.	131.0	(.	125.2)	.	140.5	-		.
			69.0		*0.1*		*20.0*			
4.A.9	14	.	131.0*	(.	116.0)	.	139.0	-		.
			80.5		*0.2*		*18.0*			
4.A.10	16	.	130.5*	-		.	138.5	-		.
			84.0				*16.5*			
4.A.11	18	.	131.0	-		.	136.0	-		.
			80.0				*17.0*			

Abbreviations: Cr-Crystalline phase; B_2'-Polar homochiral smectic phase with tilted molecules; B_7'-Switchable B_7 phase showing bistability; B_2- Polar smectic phase with tilted molecules in the layers; I-Isotropic phase; * Sample has crystal-crystal transition; enthalpy denoted is the sum of all such transitions; ( ) Monotropic transition.

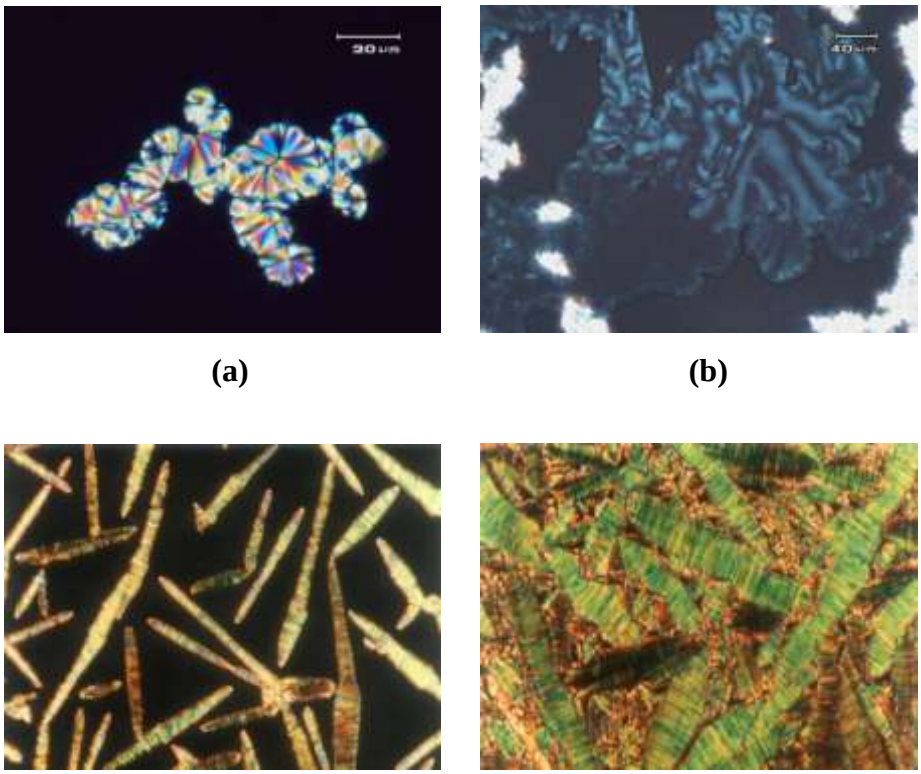

(a) **(b)**

(c) **(d)**

Figure 4.2: Photomicrographs showing typical textures. Top row: compound 4.A.2, (a) In an ordinary glass plate, T=141˚C; (b) in a substrate treated for homeotropic alignment, T=135˚C. Second row: compound 4.A.5 in an ordinary glass slide, (c) T=142˚C; (d) T=135˚C.

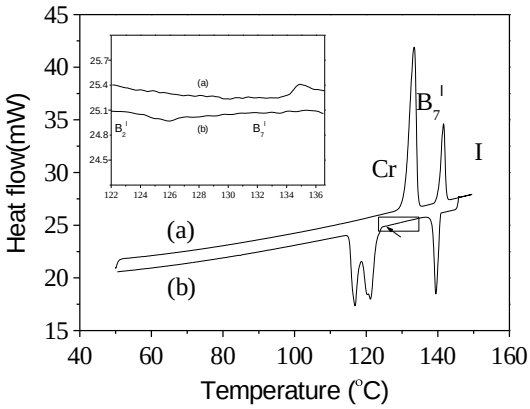

Figure 4.3: DSC thermogram of a sample of compound 4.A.8. (a) Heating cycle; (b) cooling cycle; rate 5°C min^{-1}. The transition between the two states is indicated by an arrow; inset shows the expanded region of this transition.

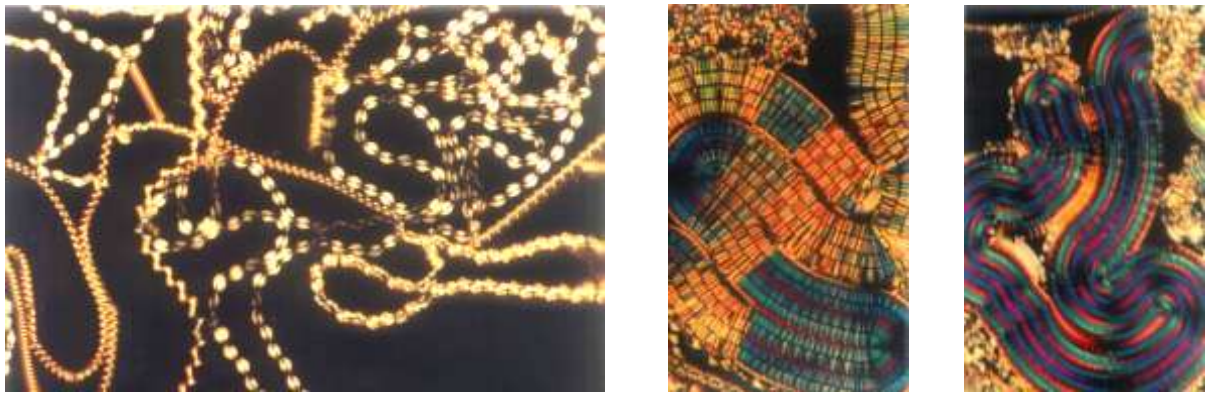

(a) **(b)** **(c)**

Figure 4.4: (a) A texture of the helical filamentary growth pattern obtained on cooling the isotropic liquid of compound 4.A.7, T= 139.8°C; (b) and (c) other beautiful textures obtained on slow cooling the isotropic liquid of compound 4.A.7, T=139°C.

On cooling the 8 μm thick sample of compound **4.A.7** a clear textural transition at 128˚C was observed wherein the focal-conic domains disappear and a finger-print texture appears as shown in figure **4.5a** and **b** respectively. Similar behaviour was observed for compounds **4.A.8** and **4.A.9**. However, this transition does not show up in the textures of 5 μm thick films as shown in figure **4.5c** and **d** respectively.

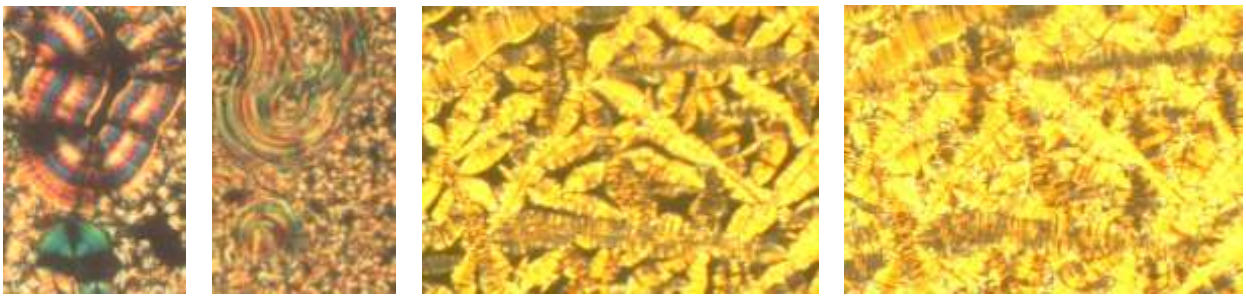

(a) **(b)** **(c)** **(d)**

Figure 4.5: Textures observed in 8 μm and 5 μm thick films on cooling the isotropic liquid of compound 4.A.7 without the application of any field. (a) 8 μm Film at 135˚C; (b) 8 μm film at 128˚C; (c) 5 μm film at 135˚C; (d) 5 μm film at 128˚C.

The textures observed on cooling under strong electric field also show a clear difference between the phase above and below 128˚C even for the 5 μm cell. This unambiguously proves the existence of two mesophases, and these have been tentatively labelled as B_7' for the higher temperature phase and B_2' for the lower temperature phase.

The mesophase exhibited by compounds **4.A.10** and **4.A.11** is the same and the textures shown by these are completely different from those of the lower homologues. For example, on slow cooling the isotropic phase of compound **4.A.10**, an unusual texture develops and in some other regions of the same sample circular domains could also be seen as shown in figure **4.6a** and **b** respectively. Although these textures are reminiscent of those seen for some columnar phases, XRD data indicates a lamellar phase. On the basis of experimental observations (described later), this mesophase has also been characterized as a B_7' phase.

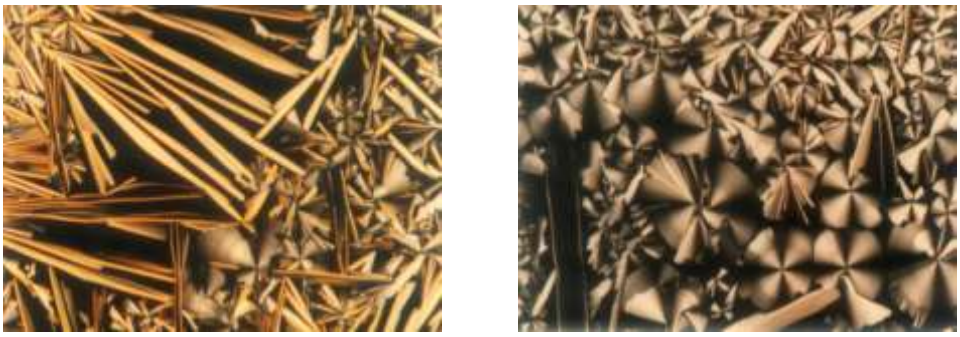

(a) **(b)**

Figure 4.6: Textures obtained for compound 4.A.10 sandwiched between an ordinary glass slide and a cover slip. (a) and (b): Different regions of the same sample obtained on slow cooling of the isotropic liquid, T=138˚C.

A plot of transition temperature versus the number of carbon atoms in the terminal chain obtained for this homologous series is shown in figure **4.7**.

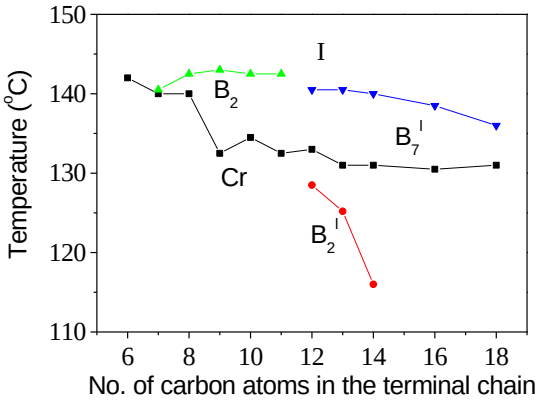

Figure 4.7: A plot of transition temperature as a function of the number of carbon atoms in the terminal chain for compounds of series 4.A.

In order to obtain more information on the phase structures, X-ray measurements were carried out on mesophases obtained on cooling the respective isotropic liquids. The diffraction patterns of all the samples showed a diffuse peak around 4.2Å in the wide-angle region indicating a liquid-like in-plane order. In the small angle region of the patterns, several Bragg reflections were obtained which are periodic. This clearly indicates a layer ordering in the mesophase. For example, mesophase of compound **4.A.2** showed three Bragg reflections in the small angle region corresponding to distances of 37.6Å, 19.0Å and 12.7Å, which are in the ratio 1:1/2:1/3. An X-ray angular intensity profile obtained for the same sample is shown in figure **4.8**. The first order layer spacing is smaller than the measured molecular length indicating a tilted director structure (the molecular length was measured considering an extended *all-trans* conformation of the chains and a bend angle of 120˚). For sample **4.A.2** a tilt angle of about 45˚was estimated using the relation $\cos\theta = d/l$ (*d*-measured layer spacing; *l*-calculated molecular length). In compounds **4.A.7-9** layer spacing was found to be temperature independent suggesting that both the mesophases are lamellar in nature. The measured layer spacing (*d* in Å) for the samples along with the corresponding Miller indices are presented in table **4.2.**

Table 4.2: The layer spacing (Å) and the corresponding Miller indices (shown in parentheses) obtained for the compounds of series 4.A.

Compound	*n*	*d*-spacing (Å)	Temperature (˚C)
4.A.2	7	37.6(01), 19.0(02), 12.7(03)	135
4.A.3	8	39.0(01), 19.9(02), 13.4(03)	138
4.A.4	9	40.7(01), 20.6(02)	130
4.A.5	10	42.9(01), 21.5(02)	128
4.A.6	11	43.5(01), 21.7(02)	125
4.A.7♣	12	45.5(01), 22.7(02), 15.2(03)	135
4.A.8♣	13	46.6(01), 23.5(02)	130
4.A.10	16	50.9(01), 25.5(02), 17.1(03)	135
4.A.11	18	53.2(01)	125

♣ The layer spacing observed remain the same in the lower temperature phase, too.

A plot of *d*-spacing (Å) as a function of number of carbon atoms in the terminal *n*-alkyl chain is shown in figure **4.9**. It is evident from the plot that, the layer spacing (*d*) increases linearly with the number of carbon atoms in the terminal chain. The increment in *d* per methylene group decreases in the higher homologues probably due to the fact that the longer chains may assume *gauche* conformation as observed in a number of long terminal chain containing calamitic mesogens.

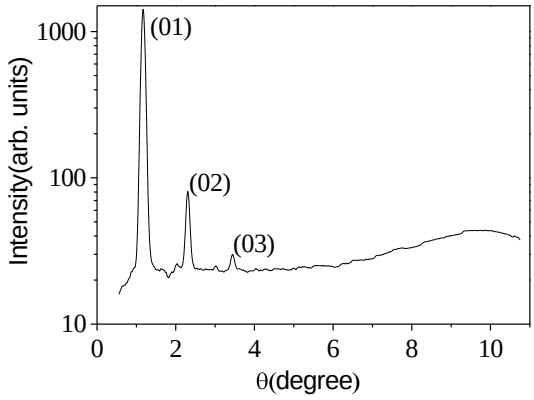

Figure 4.8: X-Ray angular intensity profile obtained for the mesophase of compound 4.A.2, T= 135˚C.

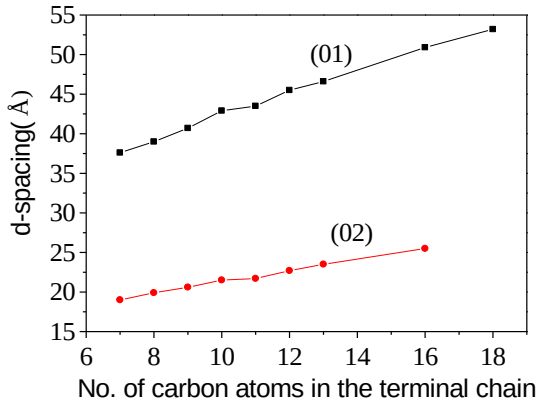

Figure 4.9: A plot of *d*-spacing as a function of the number of carbon atoms in the terminal *n*-alkyl chain for the homologues of series 4.A.

Dielectric measurements were carried out (by A. Jakli, Kent State University, Ohio, USA) on representative compounds belonging to series **4.A**. Compound **4.A.2** shows a large dielectric constant (~100) at low frequencies indicating a ferroelectric behaviour. Temperature dependence of the low-frequency (2 KHz) dielectric constant for compound **4.A.2** is shown in figure **4.10a**. The dielectric relaxation process is far from a single Debye relaxation as the Cole-Cole plot in the inset (figure **4.10b**) shows the existence of a broad range of relaxation processes with relaxation frequencies ranging between less than 100 Hz and several kHz. It should be mentioned here that the relaxation frequencies f_r, which are determined by the frequency where ε'' have maximum are also indicative of the phase. In ferroelectrics f_r<10 kHz, in antiferroelectrics f_r>100 kHz, whereas in dielectrics f_r>1 MHz.

Dielectric measurements of compound **4.A.3** indicate an antiferroelectric (AF) local arrangement, as the static susceptibility increase is small in the mesophase ($\Delta\chi$~1) as compared to the isotropic steady susceptibility (figure **4.10c** and **d**). Compound **4.A.6** has a relatively small dielectric susceptibility, $\Delta\chi$~5 (i.e., less than that for compound **4.A.2**, but larger than for compound **4.A.3**. On the other hand, the threshold field for switching E_{th} for compound **6** is less than that for **4.A.3** and larger than for **4.A.2**) in the mesophase range. The relaxation frequency range is relatively wide varying between 1 and 50 kHz (figure **4.10e** and **f**).

Dielectric spectra of a sample of compound **4.A.7** in a 5 μm cell show relaxation in 130 kHz to 35 kHz range at decreasing temperatures as shown in figure **4.11a**. This indicates antiferroelectric type in-layer ordering. The increase in ε'' above 500 kHz is electrode effect. The temperature dependence of the dielectric constants ε' and ε'' at 2 kHz is shown in figure **4.11b**. They show only one phase between the clearing point and the crystallization which takes place at around 100°C. On heating, the melting takes place at around 131°C.

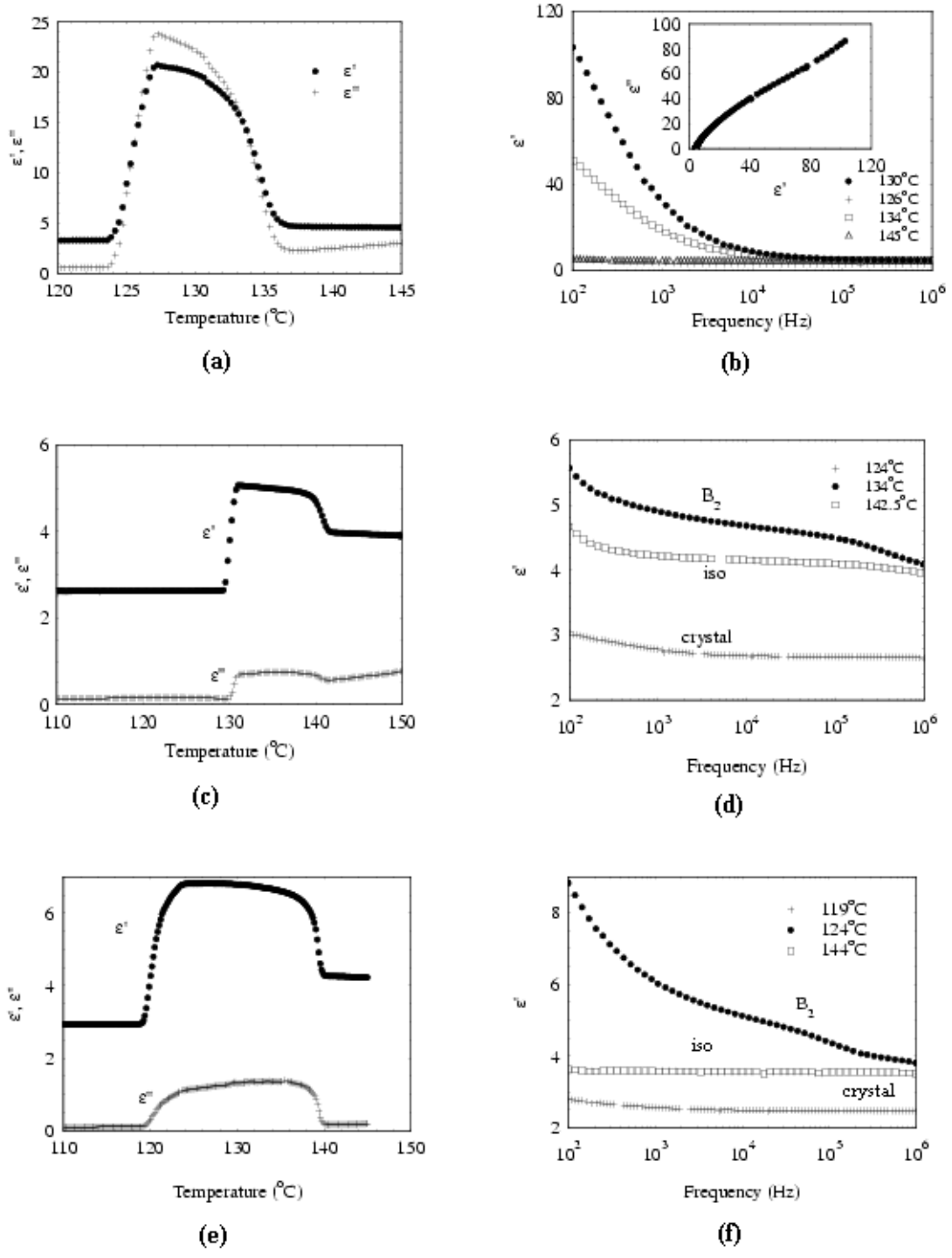

Figure 4.10: Left column (a, c, e): Temperature dependence of the low-frequency (2 kHz) dielectric constants. Right column (b, d, f): Dielectric spectra at various temperatures. Top row- compound 4.A.2; Middle row - compound 4.A.3; Bottom row - compound 4.A.6.

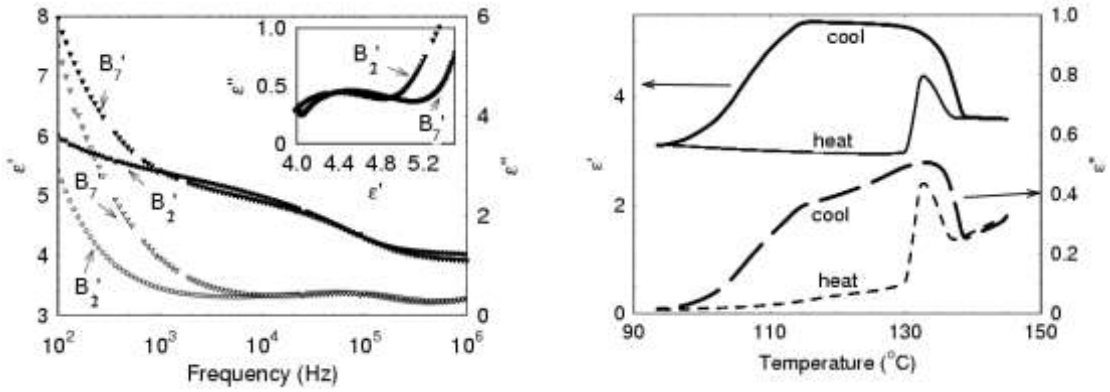

(a) **(b)**

Figure 4.11: Diagrams obtained for a sample of compound 4.A.7 in a 5 μm cell.

(a) Frequency dependence of the dielectric loss ε″ at different temperatures;

(b) temperature dependence of the dielectric constants ε′ and ε″ at 2 kHz on heating and cooling.

Electro-optical behaviour of the mesophases of compounds **4.A.2-11** was investigated in ITO coated cells of thickness 8 μm without any alignment layers employing triangular-wave and rectangular-wave electric fields as well as dc electric field. Compound **4.A.2** shows a single polarization peak under a triangular-wave electric field even at very low frequencies (~0.1 Hz) indicating a ferroelectric (FE) switching behaviour. However, the peak position is not characteristic of the one obtained in classical FE switching in which case the peak appears after the applied voltage crosses zero [22]. As can be seen in figure **4.12a,** in the present case, the peak is centered at about the zero crossing of the applied voltage. This gives an indication that the two polarization peaks of an AF state would have merged following a slow relaxation process from field induced FE to AF ground state. In order to confirm this modified triangular-wave was employed in which a time gap was introduced at zero voltage. The single peak separates into two, confirming AF behaviour as shown in figure **4.12b**. The integrated area under the curve gives a polarization value of 160 nC cm^{-2}. It is very interesting to point out here that the polarization peak appears basically without any threshold (below 0.25 Vμm^{-1}). The switching time as determined by

the positions of the polarization current maxima following fast field reversal shows approximately 1/E dependence (figure **4.12c**).

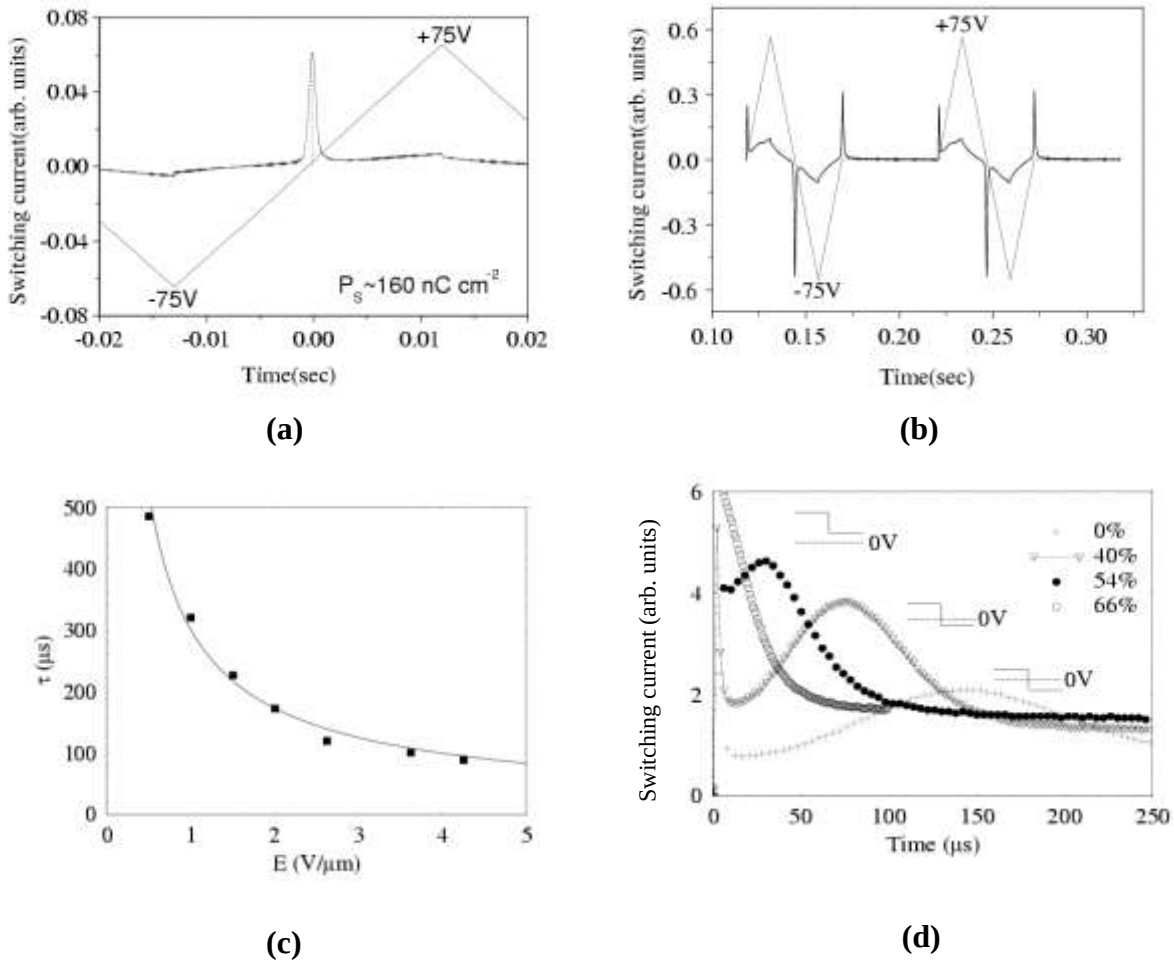

Figure 4.12: Electric current responses in the mesophase of compound 4.A.2. (a) Triangular-wave, 150V_{pp}, 20 Hz, 130˚C; (b) modified triangular-wave, 150V_{pp}, 20 Hz, 130˚C; (c) electric field dependence of the switching time at 130˚C determined from the peak positions of the time dependence of the polarization current following fast field reversal; (d) time dependence of the polarization current following step-wise field reversal with different offset fields in % of the peak – to – peak value of the reversed field.

To gain a better understanding of the nature of polarization, detailed polarization current measurements were carried out under a rectangular field with dc offsets. In case of FE switching, no polarization current is expected when the offset is over 50% of the peak-to-peak value, i.e. there is no sign inversion, whereas for AF or paraelectric situations a polarization current could be observed even in this case. As can be seen from figure **4.12d**, for material **4.A.2** polarization peaks were detected even when the offset is more than 50%. Another important feature of this graph is that both the integral area and peak position are decreasing with increasing offset.

Similar electro-optical behaviour was observed for compound **4.A.4**, too.

Compounds **4.A.3** and **4.A.5** show two distinct peaks under triangular electric field above a threshold of 5 $V\mu m^{-1}$ thus indicating an AF switching. The current response trace obtained for compound **4.A.3** is shown in figure **4.13a**. The integrated area shows a relatively low polarization value of 85 nC cm^{-2}.

The "non-perfect" peaks are probably due to an unusual kick-back effect seen in the polarization current following fast field-reversal (figure **4.13b**). This kick-back effect appears as a peak in the opposite direction after the main peak levels off. It indicates either overshooting of the director rotation or based on the small plateau after the decay of the main peak, it is a kind of backflow effect induced by the reverse polarization current.

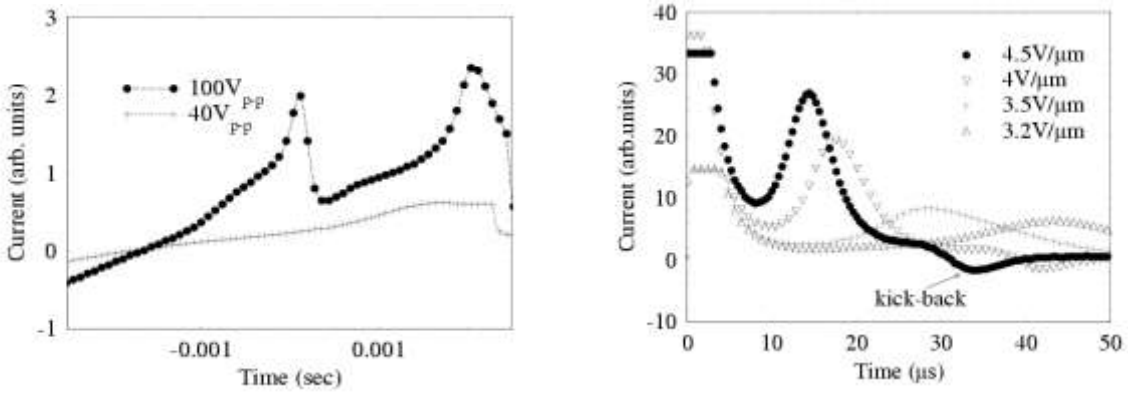

(a) **(b)**

Figure 4.13: Time dependence of polarization current at 138°C for compound 4.A.3. (a) Under triangular voltage waveforms; (b) following fast field reversal at 136°C (a negative hump after the positive one for high fields can be noticed).

For compound **4.A.6**, the time dependence of the polarization current under triangular electric field indicates ferroelectricity, since only one peak was observed even at a low frequency of about 1 Hz. This polarization peak appearing near zero electric field looks like polarization peaks obtained for helical SmC^* materials. The current response traces obtained under a triangular-wave field with a frequency of 23 Hz and 4 Hz are shown in figure **4.14a** and **b** respectively. However, the experiments employing modified triangular-wave showed two peaks per half period of the applied voltage indicating AF behaviour. The polarization reversal current at different off set values was also investigated for the mesophase of this compound. Similar to the behaviour of compound **4.A.2**, the polarization peak does not disappear at 50% of off set level. However in this case the switching time increases and broadens at off set level equal or larger than 50%, and the peak disappears above 60% off set level (figure **4.14c**). This indicates AF behaviour with threshold for relaxation from the field induced FE state back to the antiferroelectric state at about 1.2 $V\mu m^{-1}$. The FE to AF switching time, as determined from the switching time at 50% off set, ranges between 50 to 180 μs, which agrees well with the dielectrically observed range of relaxation frequencies. It is interesting to point out here that a single polarization peak was observed under triangular field down to less than a second, whereas there is relaxation to the AF state after fast field removal with relaxation time less than 200 μs. Electric field dependence of the switching time as determined from the peak position of the polarization current for the same compound is shown in figure **4.14d**.

Such a ferroelectric-like behaviour of the B_2 phase shown by compounds **4.A.2, 4.A.4** and **4.A.6** has also been observed in some asymmetric bent-core compounds reported recently [23].

When a sample of compound **4.A.7** was cooled under strong electric fields, a clear difference between the phase above and below 128˚C even for the 5 μm cell could be seen as a change in the texture and this is shown in figure **4.15a** and **b**. The temperature dependence of the transmittance of the sample of compound **4.A.7** in a 5 μm film shows smooth variation at zero field, but indicates a clear transition at 128˚C, when the material is cooled under an electric field of 13 $V\mu m^{-1}$ as shown in figure **4.15c**. It could also be observed in figure **4.15c** that the isotropic-smectic transition temperature is higher when the sample is cooled under an electric field. A plot of the electric field dependence of the shift of phase transition temperature ΔT is shown figure **4.15 d**. It can be seen that ΔT is proportional to the electric field, which indicates the presence of ferroelectric polarization that forms along the electric field.

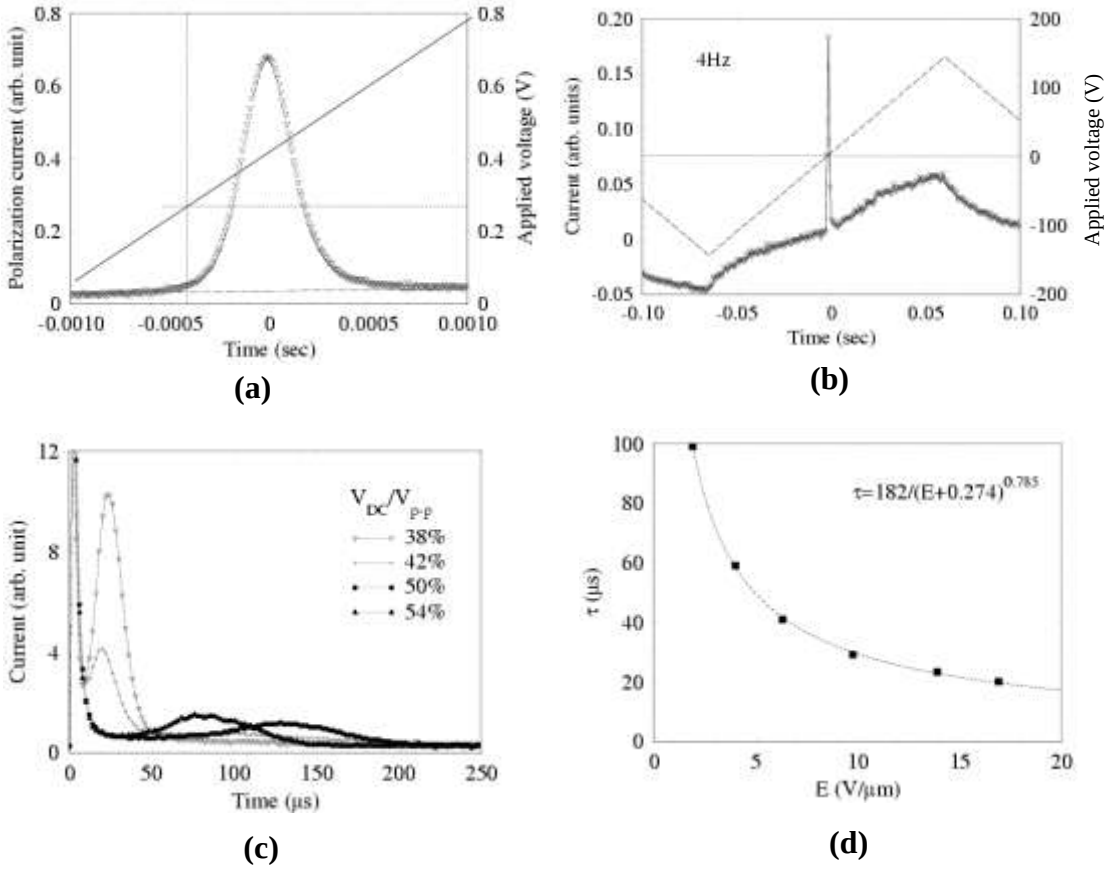

Figure 4.14: Polarization measurements on compound 4.A.6 at 136˚C. (a) 23 Hz; (b) 4 Hz, P~ 60 nC cm^{-2}; (c) polarization current under rectangular fields with off set. The peak-to-peak value of the rectangular field is 14.5 Vμm^{-1} for all cases; (d) electric field dependence of the switching time as determined from the peak position of the polarization current.

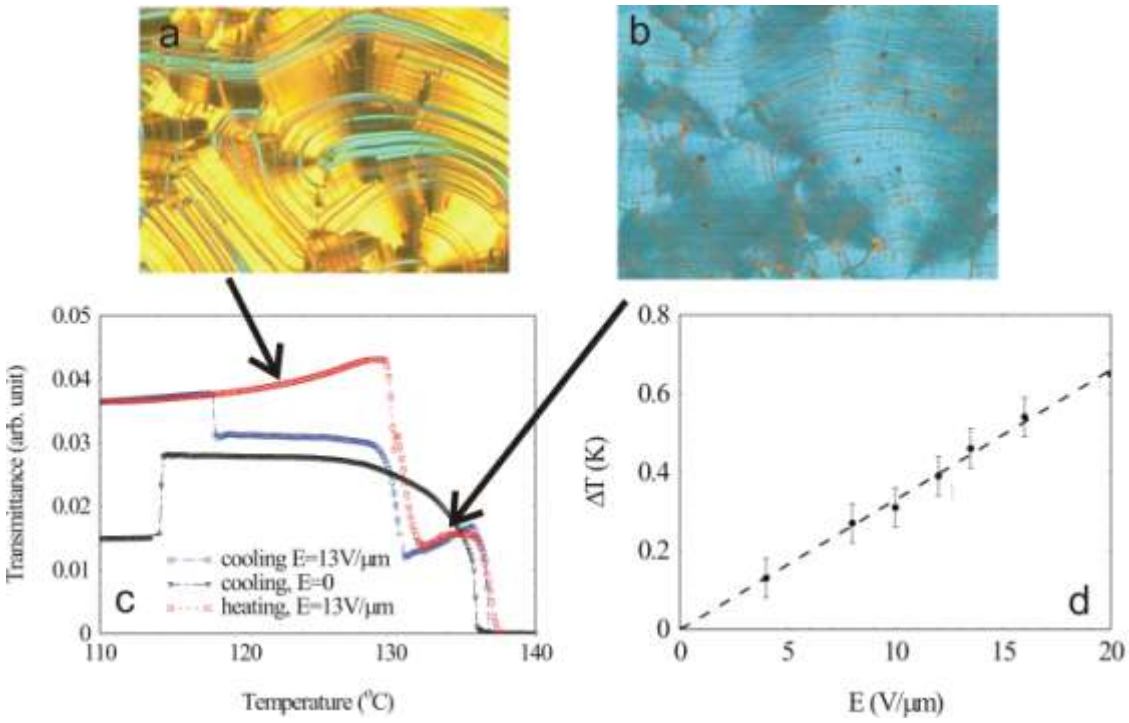

Figure 4.15: (a) Texture of compound 4.A.7 obtained by applying a rectangular electric field of 13 Vμm^{-1}, 34 Hz at 128°C; (b) at 133°C; (c) transmittance as a function of temperature on heating and cooling, at zero field and under 13 Vμm^{-1}, 34 Hz; (d) shift of the phase transition temperature as a function of the amplitude of the applied field.

On applying a rectangular voltage above about 6 Vμm^{-1}, needle like domains develop in the B_7' phase (figure **4.16a**), which rotate about their long axes (similar observations were made by Rauch *et al.* [4] on another material), but they do not change the birefringence or optic axis up to a field strength of about 12 Vμm^{-1}. Switching off the field at this stage results in a relaxation to the original low birefringence state. Above 12 Vμm^{-1} the birefringence of the needles increases (color changes to blue), and the domains start to glue together. Above 15 Vμm^{-1} field, the needles become glued together and a relatively smooth texture forms, where the optic axis rotates with the sign of the electric field and this is shown in figure **4.16b** and **c**. This state is bistable, i.e., the

optic axis stays and the birefringence changes only slightly (blue changing to violet, shows a decrease of the birefringence) after field removal as shown in figure **4.16d**. These indicate polar nature of the switching, but interestingly no polarization peak could be observed during this switching process (described later).

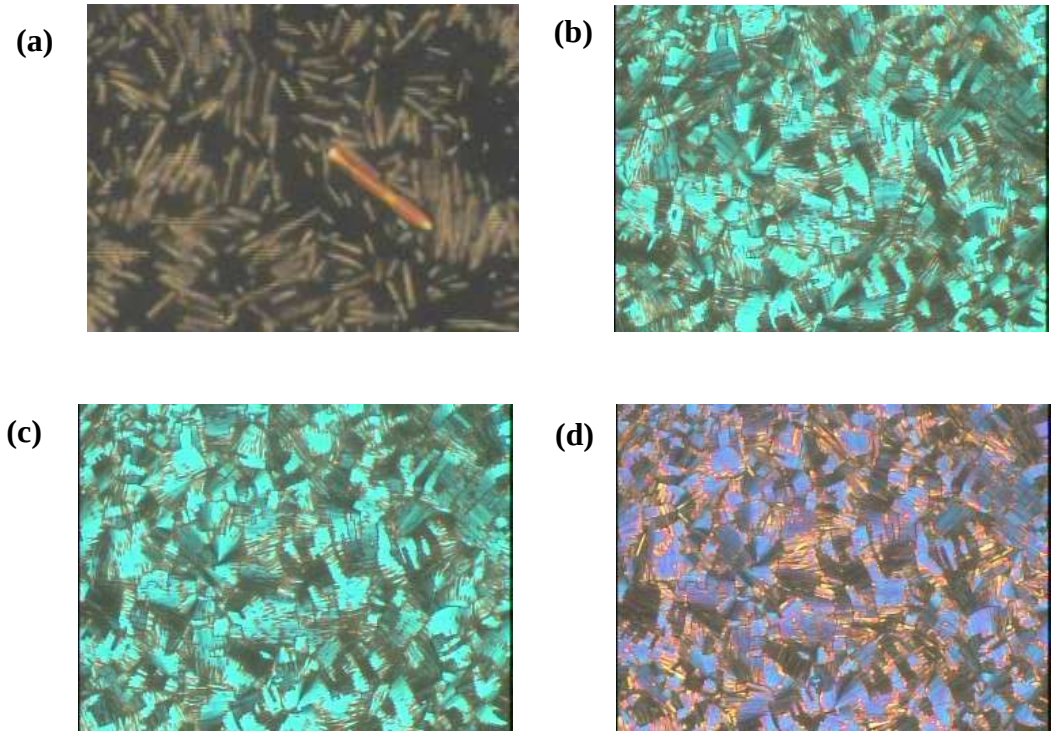

Figure 4.16: Electro-optical observations in the B_7' phase. (a) E=12 $V\mu m^{-1}$, f=13 Hz, T=136°C; (b) and (c) E= +18 $V\mu m^{-1}$ and E= -18 $V\mu m^{-1}$, T=132°C; (d) E=0 after turning off from E= -18 $V\mu m^{-1}$.

The switching in the B_2' phase was also found to be quite complex (figure **4.17**). When cooled from B_7' phase at fields above 12 $V\mu m^{-1}$ the switching between high birefringent states prevail, but it is not bistable. A smooth yellow (low birefringence) texture forms after switching off the field. This behavior can be understood in terms of a chiral antiferroelectric texture, i.e., SmC_aP_A at zero field which becomes SmC_sP_F under a strong field. However, if the strong rectangular field was maintained over a period of time, the texture transforms eventually (in about 10 minutes) to the low birefringent texture that does not show rotation of the optic axis. The same

scenario occurs when the material was cooled from the B_7' phase at zero field. At zero field some stripes could be observed, as is usual for a synclinic structure, but now it does not result in high birefringence, which shows that the synclinic tilt plane is parallel to the smectic layers.

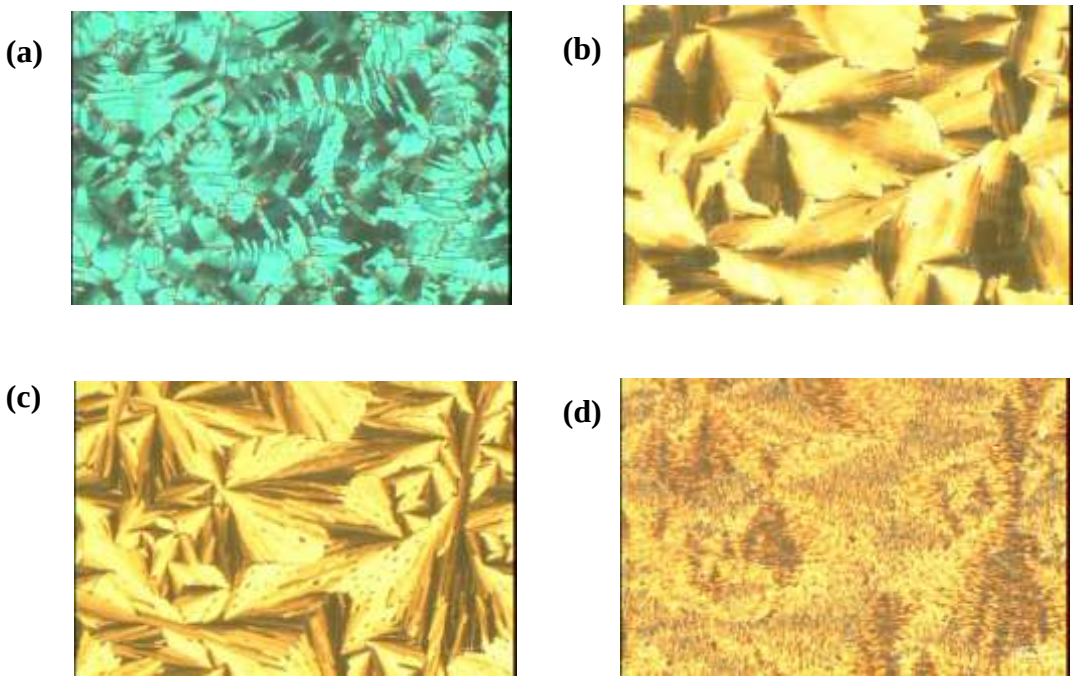

Figure 4.17: Electro-optical switching in the B_2' phase. (a) On cooling from the B_7' phase under application of a field of 12 $V\mu m^{-1}$, T=125°C; (b) the texture after turning off the field (same area as in a); (c) a field of 12 $V\mu m^{-1}$ is on for a long time; (d) E=0 after prolonged field application.

For further understanding of the phase structure, polarization current measurements were carried out under a triangular-wave electric field. The typical results are shown in figure **4.18**. In the B_7' phase, till 40 $V\mu m^{-1}$ no polarization current peak was observed (figure **4.18a**). But interestingly a bistable linear electro-optical switching was observed. In the B_2' phase, an antiferroelectric type double peak appears (figure **4.18b**, P_S ~55 nC cm^{-2} at 126°C) at a much lower threshold field (about 9 $V\mu m^{-1}$) than the threshold for the bistable linear electro-optical switching observed in the B_7' phase. This polarization current curve does not change although a

textural change was observed on prolonged application of field (figure **4.17c**) indicating that the stable B_2' phase is also antiferroelectric. Similar behaviour was observed for compounds **4.A.8** and **4.A.9** also.

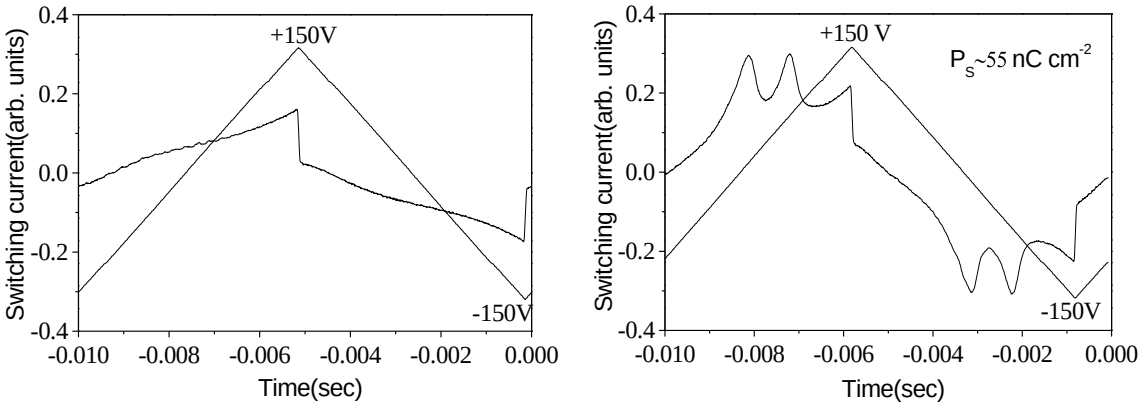

Figure 4.18: Time dependence of the polarization current in the B_7' and B_2' phases (a and b, respectively).

The mesophase of compounds **4.A.10** and **4.A.11** did not show any polarization current response under triangular electric field up to 40 $V\mu m^{-1}$. The optical observations under polarizing microscope were similar to the B_7' phase of compound **4.A.7**.

The observations made for compound **4.A.7** revealed a complex and temperature dependent transitions of these symmetric and relatively simple materials. The B_2' phase has chiral SmC_aP_A structure, which shows chiral switching for a while when cooled from the B_7' phase. As a function of time however, it relaxes to a synclinic (racemic) antiferroelectric structure. An even more extraordinary feature of these observations is that of linear electro-optical switching without observable polarization current peak (electroclinic - type switching) and the simultaneous bistability observed in the thermal range of the B_7' phase.

This behavior could be explained by the modulated in-plane polarization model [17]. According to this model the smectic layers consist of stripes (polarization splay defects) with periodicity below optical wavelength where the direction of the polarization varies up to 180˚.

This structure has no long-range azimuthal order or net polarization in the absence of electric field. However application of the electric field distorts the polarization structure of the defect array and leads to a large electroclinic effect. Since the net polarization is proportional to the applied electric field, under a triangular field this would give only a linear contribution to the electric current, which would be indistinguishable from the Ohmic current. The large electroclinic effect observed in chiral calamitic SmA* materials have already been explained by a modulated polarization structural model by Meyer and Pelcovits [24]. The bistability that has been observed above a threshold can also be explained by assuming a field-induced unwinding of the modulated structure. Just as in the case of short pitch SmC* samples, the reformation of the modulated structure would require modulation, thus the texture would remain stable after turning off the field. This bistability, however would necessarily involve switching of the polarization in reversed electric field, which would show up as peak in the polarization current measurements. This peak was clearly not present in a wide voltage range where the bistability (optic axis remains stable after field removal) was observed. In addition, similar to that of Goldstone mode of helical SmC* materials one would expect a large (ε~50) dielectric constant

$$(\Delta\varepsilon_G = \frac{1}{8\pi\varepsilon_o K}\left(\frac{pP}{\theta}\right)^2,$$

where P ~ 0.002 C m^{-2} is the spontaneous polarization, K ~ 10^{-11}N is the relevant distortion elastic constant, p ~ 0.1 μm is the periodicity and θ ~ 0.5 rad is the tilt angle) with low (f_r ~ 10kHz) relaxation frequency

$$(f_r \sim \frac{4\pi^2 K}{\gamma p^2},$$

where γ ~ 1 Pas is the rotational viscosity). Instead, a small ($\Delta\varepsilon$ ~ 2) contribution of the dielectric constant was observed that relaxes only in the 100 kHz range. To get the observed $\Delta\varepsilon$ and f_r values, about 4 times smaller modulation periodicity has to be assumed. This however would clearly show up in the small angle X-ray diffractogram in the form of multiple peaks separated by about 0.01 Å^{-1} wave numbers [17], which could not be found in the limitation of the X-ray set-up used.

It is also possible to consider another model, which assumes an out-of-layer polarization component (SmC_G structure). To describe this model the geometry shown in figure **4.19** is used. The long axis (the line connecting the end points of the average molecules) makes an angle θ with

the layer normal, which is set along the z-axis. The molecular plane is described by the azimuth angle ϕ. $\phi = 0$ or π corresponds to the SmCP (B_2) phase, whereas $0 < \phi < \pi$ describes the SmC_G phase, with chirality changing sign at $\phi = -\pi/2$ and $\pi/2$.

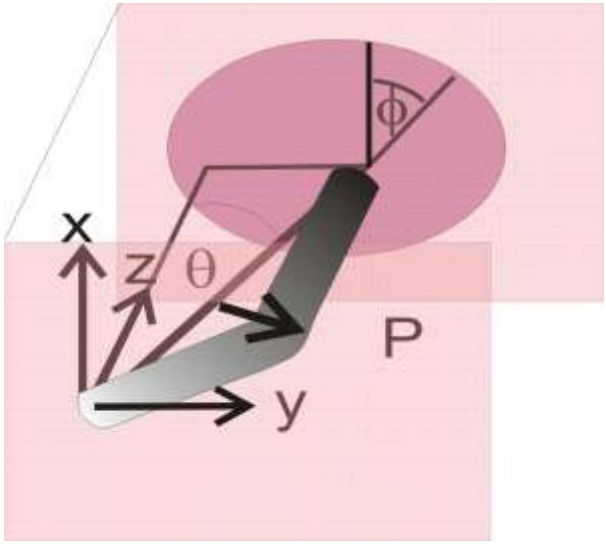

Figure 4.19: Director and layer structure of the double tilted SmC_G phase of bent-core molecules.

The low birefringence in the higher temperature phase at zero electric field indicates that the tilt is anticlinic, i.e., the sign of θ alternates from one layer to the other. When $0 < \phi < \pi$, the out-of-plane polarization results in a torque on the electric field applied across the cell along the smectic layers. When the layers are fully formed, they can be considered rigid typically below 10 $V\mu m^{-1}$ field, however the direction of the polarization can be rotated with respect to the layers by rotating ϕ closer to $\pi/2$. In order to keep the layer spacing, the component of the tilt along the film and normal to the electric field has to increase. This also results in an electro-clinic type switching. In this case however, when the field is turned off, ϕ can relax back to the original ϕ_o just by rotation around the long axis, so that the tilt angle component along the film surface (i.e. the optical axis) may remain the same, and only the birefringence decreases slightly, just as found experimentally. Remarkably, this model can also account for the rotation of the smectic layers upon field reversal (figure **4.16**) and can be explained as follows. In different domains, where P_{op}

points in opposite directions, the switching would require opposite rotation of the layers, which results in the breaking of the layers to needles with long axis parallel to the layers, as observed experimentally (figure **4.16a**).

Finally, the transition from the needle-like inhomogeneous texture to the smooth continuous texture above a second threshold field $E_2 \sim 18$ $V\mu m^{-1}$ could also be explained and is very similar to that observed [4] earlier for a fluorinated material. Just as in that case, here also this might correspond to a field induced SmC_G-SmCP transition. At this transition the second tilt angle becomes $\phi=\pi/2$, i.e., the out-of-plane polarization component becomes zero, which means a transition to the B_2 phase with C_2 symmetry. In this thermal range the switching does not require any rotation of the layers, thus resulting in the observed smooth texture.

It is appropriate to mention here that the transition from an inhomogeneous structure to a smooth one can also be accounted by the modulated polarization model, as the transition where the modulation disappears. The only difference is that the bistability and the absence of the polarization peak cannot be explained assuming only in-plane polarization components.

It is important to point out here the influence of an applied electric field to the mesophase structure of the bent-core compounds. Infact, Bedel *et al.* [7] carried out a fairly detailed investigation of the influence of an applied electric field on the phase behaviour of a series of compounds. They show that (for a particular homologue) at zero voltage only one phase is seen while on increasing the field at elevated temperatures, two different phases are observed at two different threshold voltages and these phase transitions are reversible. Similarly, Ortega *et al*. [25] found a field induced transition from a Col_r to a $SmCP_A$ phase, which was found to be reversible. Recently we have reported [26, 27] field induced irreversible columnar to smectic phases as well as racemic to homochiral smectic phase transitions. Such effects were also observed [4, 28] earlier and a summary of the effect of electric field on the mesophase structure can be found in an excellent review [18].

DC field experiments were also carried out in order to gain a better understanding of the switching behaviour of the mesophase. Polyimide coated ITO glass cells of thickness 8 μm were used for the experiments. On slow cooling of the isotropic liquid of compound **4.A.2** under a field of 5.5 $V\mu m^{-1}$, circular domains were obtained in which extinction brushes are oriented along the crossed polarizers which suggests an anticlinic organization of the molecules in the mesophase. The orientation of the brushes remains same either on reversing the field or on removing the field.

However, a slight decrease in the birefringence was observed on switching off the field. The small difference in the birefringence between the field off and field on states can be explained by assuming that tilt direction of the anticlinic layers is different in the field off and on states. The texture obtained on turning off the field was stable for several hours. The photomicrographs obtained under these conditions are shown in figure **4.20a**. These observations indicate either a bistable switching process of FE structure, or the relaxation of the field-induced FE states to the ground state AF structure via the rotation of the molecules along their long molecular axis. Such a relaxation process preserves the orientation of the molecules (clinicity) but results in inversion of layer chirality. Although the ac field experiments (modified-triangular and rectangular fields) indicate an AF ground state, the high dielectric constant observed is not compatible with such an AF structure. To explain these observations, a structure with an anticlinic FE organization locally and an AF organization macroscopically is assumed. In other words, polarization does not get cancelled out in adjacent layers as in the case of standard antiferroelectric B_2 ($SmCP_A$) phase [19], but averages out in a range that is much larger than the layer spacing *d.* Thus, during the switching process a bunch of layers (an anticlinic FE domain) reorient along the direction of field and not every other layer as in case of normal $SmCP_A$ phases. This switching process is similar to the non-classical AF switching reported recently by Keith *et al*. [29]. On the basis of this assumption, a possible molecular organization under the field and at zero field are shown in figure **4. 20c**. Thus an anticlinic ferroelectric structure (SmC_aP_F) can be considered under the field, which relaxes to an anticlinic macroscopically non-polar structure in the ground state either via the rotation of the molecules around a cone, or by randomizing the azimuth angle of the locally ferroelectric anticlinic domains. It should be mentioned here that there also exists a synclinic antipolar correlation near the boundaries of the FE domains, but on the average it is anticlinic organization, hence the orientation of the brushes are along the crossed polarizers at zero field.
Similar optical behaviour was also observed for compound **4.A.4** under dc electric field and the photomicrographs obtained under the field are shown in figure **4. 20b**.

The mesophase of compound **4.A.3** also grows in the form of circular domains on slow cooling from the isotropic state under the field. Two kinds of domains were observed (**C** and **R** in figure **4.21a**). In domain **C**, the extinction brush is tilted in a clock-wise direction with respect to the crossed polarizers, whereas in domain **R** the extinction cross is oriented along the polarizers. On reversing the polarity of the applied field, the extinction cross in domain **C** tilts in a counter

clock-wise direction but the domain **R** is unaffected. On switching off the field, the dark brushes in domain **C** orient along the polarizers and in domain **R** stripes running across the layer normal are observed.

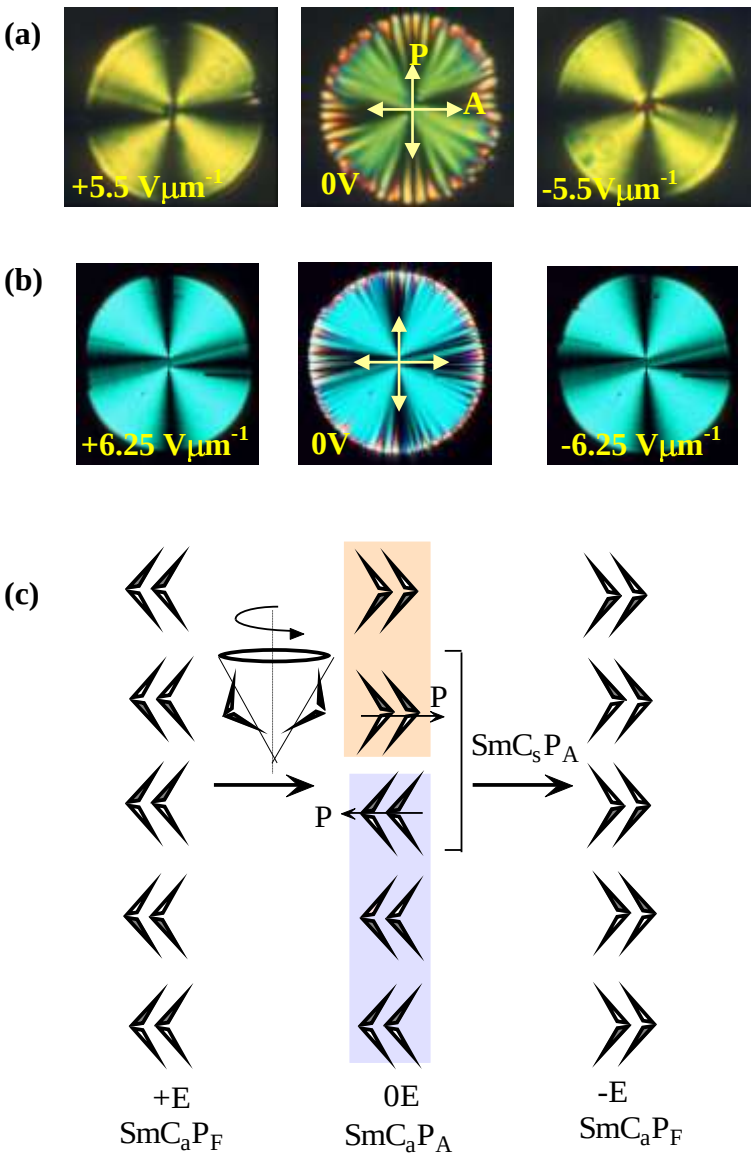

Figure 4.20: Photomicrographs obtained for the mesophase of, (a) compound 4.A.2 under dc electric field, T=140.5˚C; (b) compound 4.A.4 under dc electric field, T=142˚C. (c) Possible molecular organization for the mesophase of compound 4.A.2 and 4.A.4 under +E, 0E and –E.

These observations suggest that domain **C** is chiral with a SmC_sP_F structure under the field, which relaxes to chiral SmC_aP_A structure on removal of the field. Domain **R** represents a racemic (SmC_sP_A) structure. The molecular organizations with a schematic representation in chiral and racemic domains have been discussed in detail in Chapter 2. Compound **5** also exhibits racemic (**R**) and chiral (**C**) domains under the field and the same is shown in figure **4.21b**.

When the isotropic liquid of compound **4.A.6** was cooled slowly under the field a fan-shaped texture with extinction direction oriented along the crossed polarizers was observed. On turning off the field, stripes developed on the texture but the orientation direction of the extinction cross remained the same. This suggests a racemic antiferroelectric ground state structure similar to domain **R** described for compound **4.A.3**. However, a single polarization peak was observed for the mesophase under a triangular-wave electric field even at very low frequencies and at very low threshold voltages. On the basis of this observation an anticlinic ferroelectric local structure can be considered, where the polarization averages out in a scale larger than the layer spacing. Therefore the stripes observed at zero field could be due to this random orientation of polarization. Hence, it is difficult to predict the exact ground state structure of the mesophase of compound **4.A.6**. The photomicrographs obtained for the mesophase of compounds **4.A.6** under the field are shown in figure **4.21c**.

On slow cooling the isotropic liquid of compound **4.A.7** in a 8 μm cell into the mesophase (T=137˚C) under an applied electric field of 130V, a circular domain with extinction cross making an angle with respect to the polarizers was observed. On reversing the polarity of the applied field the extinction cross tilts in the opposite direction and remain unchanged on removal of the field, indicating a synclinic ferroelectric state (SmC_sP_F) for the higher temperature mesophase (B_7'). The bistable states thus obtained were stable for several hours. However, on cooling under the same conditions to 128˚C, and terminating the field, the extinction cross-oriented along the polarizer and analyzer directions. Hence, the switching process is clearly tristable and indicates an anticlinic antiferroelectric state (SmC_aP_A) for the lower temperature phase (B_2'). The bistable switching circular domains obtained for compound **4.A.7** at 137˚C and the tristable switching circular domains obtained at 125˚C are shown in figure **4.22**. Similar results were obtained for compounds **4.A.8** and **4.A.9** also.

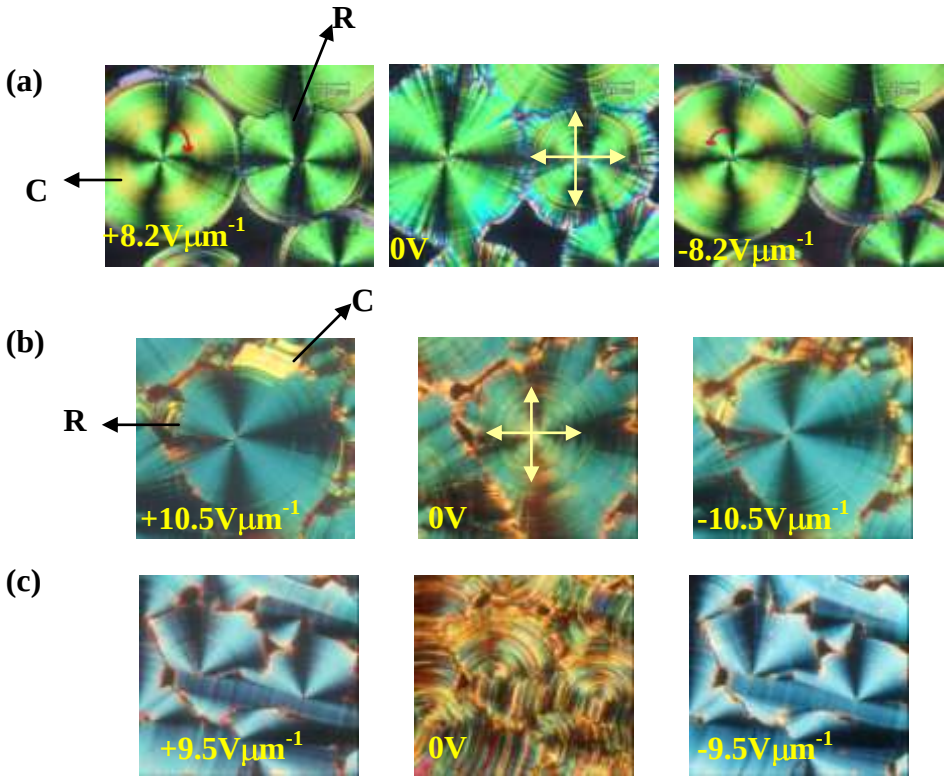

Figure 4.21: Photomicrographs showing the textures of, (a) compound 4.A.3, T=141.5˚C; (b) compound 4.A.5, T=140˚C; (c) compound 4.A.6, T=139˚C, under dc electric field.

The phase behaviour of compounds **4.A.10** and **4.A.11** under dc electric is similar. For example, on slow cooling a sample of compound **4.A.10** from the isotropic state under a dc electric field of 12 $V\mu m^{-1}$ the mesophase develops in the form of dark and bright domains, which reverse on reversing the polarity of the applied field. However, removal of the field does not affect the texture, except for a small change in the birefringence. This bistable switching indicates FE behaviour for the mesophase. But interestingly, no polarization peak was observed during the switching process on application of a triangular-wave electric field. Similar observations were made for compound **4.A.11**, too. This switching process is very similar to the linear bistable switching observed for the B_7' phase of homologues **4.A.7-9**, hence, the same structure can be

assumed for the mesophase of compounds **4.A.10** and **4.A.11**, as well. Textures of the B_7' phase of compound **4.A.10** obtained under the field and at zero field are shown in figure **4.23**.

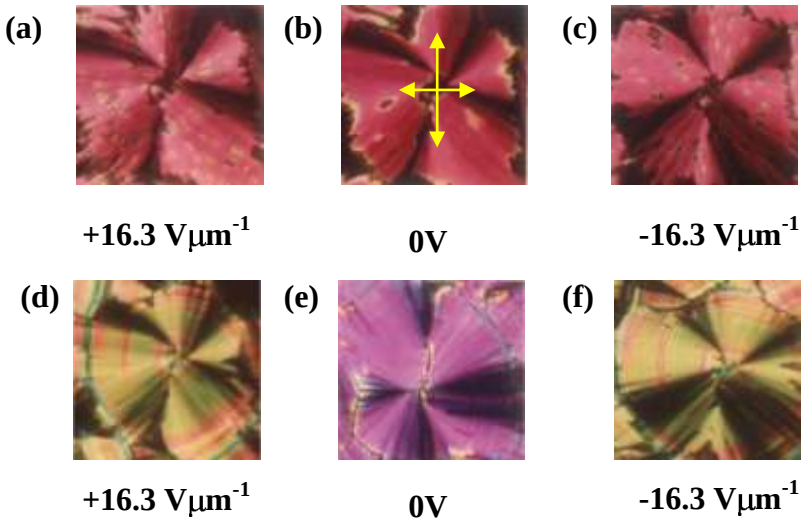

Figure 4.22: (a), (b) and (c) Bistable switching domains (SmC_sP_F) obtained in B_7' phase, T=137°C; (d), (e) and (f) tristable switching domains (SmC_aP_A) obtained in the B_2' phase, T=125°C by applying dc voltage.

Figure 4.23: Textures of the B_7' phase of compound 4.A.10 obtained under dc electric field, T=128°C. (a) +12 V μm^{-1}; (b) 0V; (c) -12 V μm^{-1}.

Part II

In this part the synthesis and mesomorphic properties of a homologous series of compounds (series **4.B**) in which the orientation of the azomethine linkage group in compounds discussed in Part I has been reversed, are described. The general molecular structure of the compounds investigated is shown below (structure **4.2**).

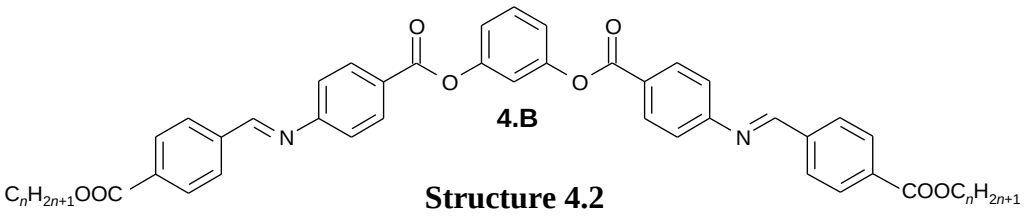

Structure 4.2

Synthesis

The general synthetic pathway used to prepare the new symmetrical bent-core compounds is shown in scheme **4.2**. 4-Formylbenzoic acid and 4-aminobenzoic acid were obtained commercially and used without further purification. Commercially obtained resorcinol was purified by column chromatography followed by crystallization. 4-Formylbenzoic acid was reacted with an appropriate *n*-alcohol in the presence of *N*, *N*′-dicyclohexylcarbodiimide (DCC) as dehydrating agent and 4-(*N*, *N*- dimethylamino)pyridine (DMAP) as catalyst to obtain *n*-alkyl 4-formylbenzoate, which was then condensed with 4-aminobenzoic acid to obtain 4-(4-*n*-alkyloxycarbonylbenzylideneamino)benzoic acid. The five-ring bent-core compounds were prepared by esterification of this bis carboxylic acid with resorcinol.

Results and discussion

The transition temperatures and the associated enthalpy values obtained for this series of compounds are summarized in table **4.3**. In this series, only six compounds were prepared and the lower homologues were not prepared because compound **4.B.1** with *n*-decyl chain did not show any mesophase. The other five homologues exhibit a metastable mesophase whose optical textures

are all similar. When a sample of compound **4.B.4** was cooled from the isotropic phase, the mesophase appeared as fractal nuclei, which coalesce to form a weakly birefringent texture.

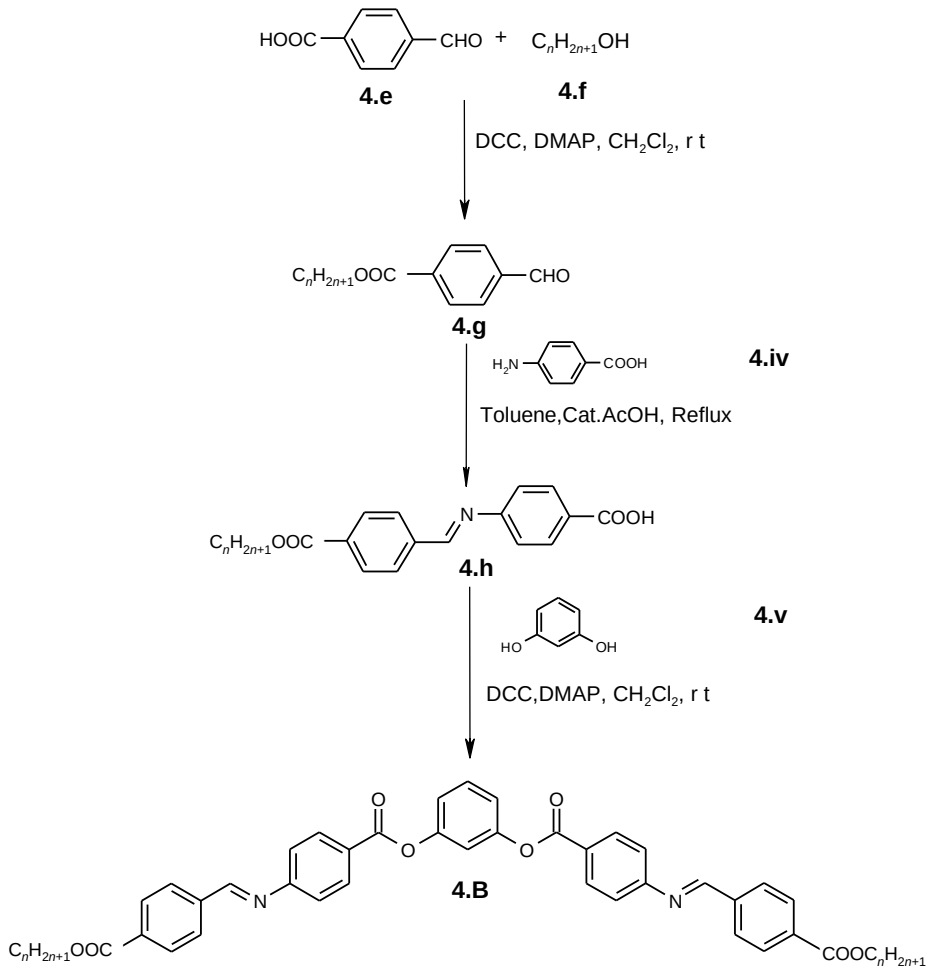

Scheme 4.2: Synthetic route employed for the preparation of the bent-core compounds, 4.B

However, on rotating the polarizer (or analyzer) by 7˚ from the crossed position, bright and dark domains could be distinguished. By rotating the polarizer in the opposite direction, bright domains become dark and *vice versa*. This observation suggests that bright and dark domains correspond to chiral domains of opposite handedness, which exhibit the opposite sign of optical rotation. Photomicrographs obtained with these chiral domains are shown in figure **4.24**.

Table 4.3: Transition temperatures (˚C) and the associated enthalpy values (kJ mol^{-1}, in italics) for the compounds of series 4.B.

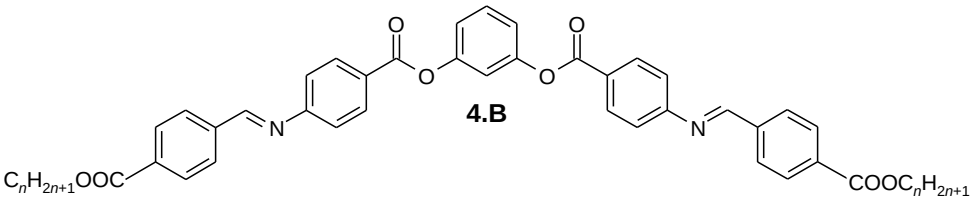

Compound	*n*	Cr		$SmCP_A$		I
4.B.1	10	.	139.5*	-		.
			73.0			
4.B.2	11	.	137.5	(.	120.0)	.
			69.0		*16.5*	
4.B.3	12	.	136.0*	(.	120.5)	.
			72.0		*15.0*	
4.B.4	14	.	133.0*	(.	121.0)	.
			120.4		*18.3*	
4.B.5	16	.	132.5	(.	121.0)	.
			131.5		*18.5*	
4.B.6	18	.	130.5*	(.	119.0)	.
			134.2		*16.6*	

Abbreviations: See table **4.1**, $SmCP_A$- Polar smectic C phase with antiferroelectric switching behaviour.

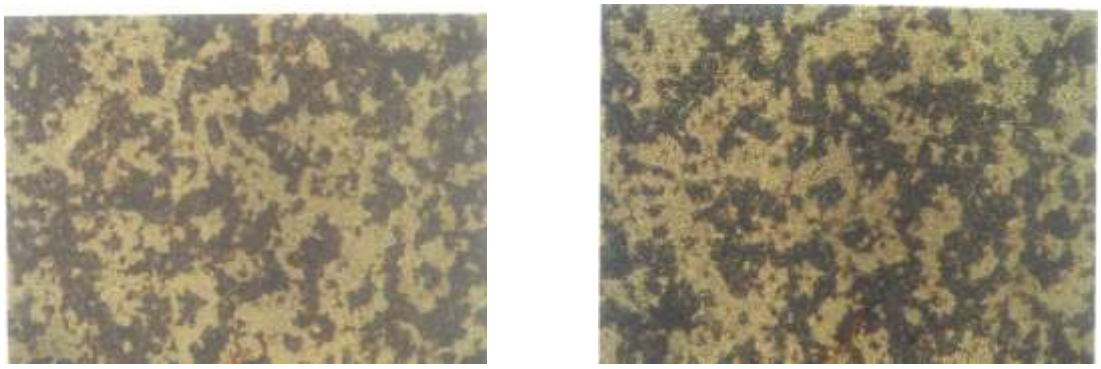

(a) **(b)**

Figure 4.24: Chiral domains of opposite handedness obtained for the mesophase of compound 4.B.4 (T=119˚C) by rotating the analyzer from crossed position by (a) +7˚ and (b)-7˚ respectively.

The observation of textures showing domains of opposite handedness were first reported by Thisayukta *et al*. [30, 31] and Heppke *et al*. [15b]. Soon, compounds exhibiting similar patterns were reported [32] by Murthy and Sadashiva and on the basis of XRD results and electro-optical investigations, the mesophase was characterized as $SmCP_A$. Subsequently, the observation of such textures for SmCP phases has been made in a number of other systems also [33-41]. The mesophase of remaining homologues, **4.B.2**, **4.B.3**, **4.B.5** and **4.B.6** exhibit similar textures and have all been characterized as $SmCP_A$ phase (electro-optical studies described later). A plot of transition temperature as a function of the terminal chain length for this homologous series is shown in figure **4.25**. The clearing points fall on a smooth curve whose slope is similar to those seen earlier for the $SmCP_A$ phase observed in various other homologous series of compounds [32].

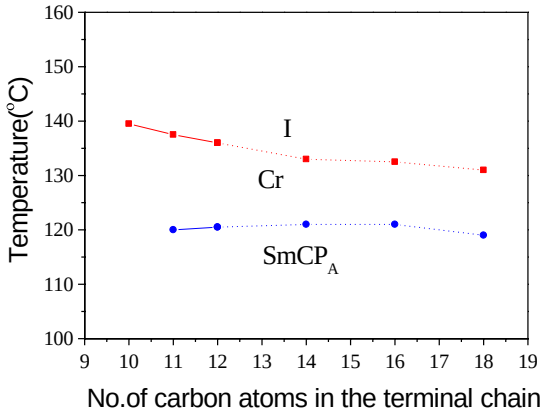

Figure 4.25: A plot of transition temperature as a function of the number of carbon atoms in the terminal chain for compounds of series 4.B.

XRD measurements could not be carried out on the mesophase of these compounds as the sample crystallizes quite rapidly. However, electro-optical measurements were carried out close to the clearing temperature. ITO coated transparent cells, which were treated for planar alignment (EHC, Japan) with a cell gap of 8 μm were used for the experiments. The cell was filled with the sample in its isotropic phase by capillary action. For example, when a sample of compound **4.B.4** was cooled from the isotropic phase under a triangular-wave electric field of $60V_{pp}$, 100 Hz, at 119˚C a single peak per half period was observed. However, this single peak splits into two on

reducing the frequency to 5 Hz, indicating an antiferroelectric switching behaviour. The switching current response obtained at $150V_{pp}$ and 5 Hz is shown in figure **4.26**. The calculated polarization value was found to be 30 nC cm^{-2}, which is quite low for a $SmCP_A$ phase. This is probably due to the fact that measurements were made close to the clearing temperature.

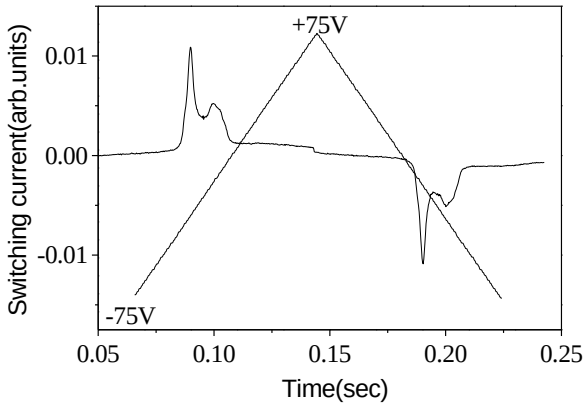

Figure 4.26: Switching current response obtained by the application of triangular-wave electric field for a sample of compound 4.B.4 at $150V_{pp}$; 5 Hz; T=119˚C.

It is interesting to point out here that three postulates have been proposed in explaining the dark texture composed of chiral domains of opposite handedness exhibited by the $SmCP_{F/AF}$ mesophases of bent-core compounds.

Ortega *et al*. [38] have explained the origin of chirality and hence optical activity in homochiral antiferroelectric phases (SmC_aP_A) by considering a helicoidal structure with the pitch equal to twice the smectic layer ordering. The helicoidal arrangements of the small domains are assumed to be randomly oriented giving rise to optical isotropy and an averaged optical activity.

Hough *et al*. [42] have proposed that the optical activity is entirely due to layer chirality and they demonstrated that the uniform stacking of chiral layers can lead to a significant collective optical rotation, even in the absence of any chiral superlayer structure such as, a helix.

Another explanation [18] is based on the segregation of chiral conformers. They propose a helical structure composed of slabs with helix axis parallel to the layers (TGB-like), similar to the structure of B_4 phase. They consider the fact that in a confined geometry of a layer structure, molecules with uniform chirality sense of the conformers can pack more efficiently than the

conformers with an opposite chirality sense thus giving rise to a spontaneous separation of the enantiomeric conformers into distinct regions.

Conclusions

Two homologous series of novel five-ring bent-core compounds containing *n*-alkyl carboxylate groups in the terminal positions have been investigated. In series **4.A**, the lower homologues (compounds **4.A.2-6**) exhibit a macroscopic antiferroelectric B_2 phase. The middle homologues (compounds **4.A.7-9**) exhibit two mesophases: the lower temperature one is classified as a B_2' phase and it shows a SmC_aP_A structure, whereas the higher temperature phase is characterized as a B_7' phase, which is bistable and shows analogous linear electro-optical switching. The homologues **4.A.10** and **4.A.11** exhibit only a single B_7' phase.

It is interesting to point out here that, although the mesophase observed in the lower homologues (compounds **4.A.2-6**) is macroscopically non-polar, an odd – even type alteration of the nanoscopic director organization can be observed as a function of the number of carbon atoms (*n*) in the terminal chains. The mesophases of compounds **4.A.2, 4.A.4** and **4.A.6** (*n*=7, 9 and 11, respectively) appear to have a locally anticlinic FE structure and the polar order averages out in a range much larger than the layer spacing *d*. However, the mesophase of compounds **4.A.3** and **4.A.5** (*n*=8 and 10, respectively) show normal antiferroelectric structure with a synclinic (racemic) or an anticlinic (chiral) local layer arrangement.

The odd – even effects were also observed in the steady dielectric susceptibility and the value of the threshold voltage for polarization switching (for *n* odd - 7, 9, 11: $\Delta\chi >> 1$ and $E_{th} << 5$ $V\mu m^{-1}$, whereas for *n* even- 8, 10: $\Delta\chi << 1$ and $E_{th} >> 5$ $V\mu m^{-1}$). The differences between these parameters for the subsequent homologues decrease on ascending the series.

It is appropriate to point out here that, there is a report [43] of odd – even behaviour for the alternative appearance of ferroelectricity (when *n* is even) and antiferroelectricity (when *n* is odd) in two homologous series of bent-core compounds and this behaviour has been attributed to the difference in the interlayer steric interactions. A theoretical formula has also been proposed considering steric interaction, dipole-dipole interaction and van der Walls attraction [44]. The observed odd – even effects in the present series of compounds probably have entropic reasons. The end chain units prefer to be parallel because the out-of-layer fluctuations are allowed in this case [45]. For odd carbon atoms the end segments of the neighbouring molecules are parallel to

each other when the tilt of the molecular planes are anticlinic, whereas for even carbon atoms the end segments are parallel for synclinic situation. Although the observations show that polar order averages out on long range even for the odd homologues, the correlation length ξ_P of the ferroelectric order shows an odd – even effect, too: $\xi_P >> d$ *for n odd* and $\xi_P \sim d$ *for n even*. This is corroborated with the observed $\Delta\chi$ and E_{th} values. It could be emphasized that these odd – even effects became possible, because the materials have relatively low polarization, which means that the polar interaction does not suppress the steric effects.

All the compounds of series **4.B**, except for compound **4.B.1** (which is crystal) show a monotropic $SmCP_A$ phase which exhibit chiral domains of opposite handedness. It should be pointed out here that the compounds of series **4.B** differ form those of series **4.A** only by the way in which the azomethine linking group is attached. The present study indicates the profound influence of the orientation of the linking group on the mesomorphic behaviour.

Synthesis

***n*-Hexyl 4-nitrobenzoate, 4.b.1**

4-Nitrobenzoic acid, **4.a** (2g, 11.9 mmol), *n*-hexyl alcohol, **4.i** (1.2g, 11.9 mmol) and a catalytic amount of DMAP in dichloromethane (50 ml) were stirred for 15 minutes at room temperature. To this stirred mixture, DCC (2.7g, 13.1 mmol) was added and stirring continued for a further 2 hours. The precipitated urea was filtered off and washed thoroughly with chloroform. The filtrate was concentrated to obtain a liquid, which was passed through a column of silica gel using chloroform as an eluant. The product obtained by evaporation of the solvent from the eluate was a liquid. Yield 2.5g (84%), viscous liquid. ν_{max}: 2956, 2931, 2858, 1728, 1724, 1608, 1529, 1467, 1274, 1014 cm^{-1}; δ_H: 8.27 (d, ^3J 8.84 Hz, 2H, Ar-H), 8.19 (d, ^3J 8.88 Hz, 2H, Ar-H), 4.35 (t, ^3J 6.6 Hz, 2H, Ar-COO-CH_2-), 1.82-1.74 (quin, ^3J 6.76 Hz, 2H, Ar-COO-CH_2-$\underline{CH_2}$-), 1.45-1.27 (m, 6H, (-CH_2-)$_3$), 0.87 (t, ^3J 6.4 Hz, 3H, -CH_3); $C_{13}H_{17}NO_4$ requires C 62.14, H 6.81, N 5.57; found C 62.45, H 6.50, N 5.35 %.

***n*-Hexyl 4-aminobenzoate, 4.c.1**

Compound **4.b.1** (2.0g) in 1,4-dioxane (30 ml) and 5% Pd-C (0.4g) were stirred in an atmosphere of hydrogen at 60˚C until the reaction was complete which was monitored by thin layer chromatography using Merck 60 silica gel plates. The reaction mixture was filtered hot and the solvent was evaporated to obtain the product, which was crystallized using *n*-hexane. Yield 1.6g (90%), m. p. 60-61.5˚C. ν_{max}: 3419, 3330, 3220, 2929, 2852, 1693, 1687, 1681, 1639, 1593, 1444, 1282, 1172, 1120 cm^{-1}; δ_H: 7.85 (d, ^3J 8.64 Hz, 2H, Ar-H), 6.63 (d, ^3J 8.64 Hz, 2H, Ar-H), 4.25 (t, ^3J 6.68 Hz, 2H, Ar-COO-CH_2-), 4.03 (s, 2H, Ar-NH_2) 1.76-1.69 (quin, ^3J 6.76 Hz, 2H, Ar-COO-CH_2-$\underline{CH_2}$-), 1.42-1.26 (m, 6H, (-CH_2-)$_3$), 0.89 (t, ^3J 6.92 Hz, 3H, -CH_3); $C_{13}H_{19}NO_2$ requires C 69.97, H 8.45, N 6.18; found C 70.0, H 8.38, N 6.14 %.

***n*-Heptyl 4-nitrobenzoate, 4.b.2**

Yield 78%, viscous liquid. ν_{max}: 2956, 2929, 2858, 1726, 1724, 1608, 1529, 1467, 1350, 1276, 1114, 1103, 1014 cm^{-1}; δ_H: 8.27 (d, ^3J 8.84 Hz, 2H, Ar-H), 8.19 (d, ^3J 8.88 Hz, 2H, Ar-H), 4.35 (t, ^3J 6.6 Hz, 2H, Ar-COO-CH_2-), 1.82-1.74 (quin, 2H, ^3J 6.76 Hz, Ar-COO-CH_2-$\underline{CH_2}$-), 1.45-1.27 (m, 8H, (-CH_2-)$_4$), 0.87 (t, ^3J 6.4 Hz, 3H, -CH_3); $C_{14}H_{19}NO_4$ requires C 63.39, H 7.2, N 5.28; found C 63.21, H 6.82, N 5.50 %.

***n*-Heptyl 4-aminobenzoate, 4.c.2**

Yield 86%, m. p. 74-75˚C. ν_{max}: 3421, 3334, 3313, 3220, 2922, 2852, 1683, 1635, 1596, 1575, 1280, 1120 cm^{-1}; δ_H: 7.85 (d, ^3J 8.64 Hz, 2H, Ar-H), 6.63 (d, ^3J 8.64 Hz, 2H, Ar-H), 4.25 (t, ^3J 6.68 Hz, 2H, Ar-COO-CH_2-), 4.03 (s, 2H, Ar-NH_2) 1.76-1.69 (quin, ^3J 6.76 Hz, 2H, Ar-COO-CH_2-$\underline{CH_2}$-), 1.45-1.28 (m, 8H, (-CH_2-)$_4$), 0.89 (t, ^3J 6.92 Hz, 3H, -CH_3); $C_{14}H_{21}NO_2$ requires C 71.46, H 8.98, N 5.95; found C 71.07, H 8.90, N 5.74 %.

***n*-Octyl 4-nitrobenzoate, 4.b.3**

Yield 80%, viscous liquid. ν_{max}: 2954, 2925, 2854, 1724, 1718, 1708, 1577, 1504, 1274, 1201, 1016 cm^{-1}; δ_H: 8.27 (d, ^3J 8.84 Hz, 2H, Ar-H), 8.19 (d, ^3J 8.88 Hz, 2H, Ar-H), 4.35 (t, ^3J 6.6 Hz, 2H, Ar-COO-CH_2-), 1.82-1.74 (quin, ^3J 6.76 Hz, 2H, Ar-COO-CH_2-$\underline{CH_2}$-), 1.45-1.27 (m, 10H, (-CH_2-)$_5$), 0.87 (t, 3H, ^3J 6.4 Hz, -CH_3); $C_{15}H_{21}NO_4$ requires C 64.49, H 7.57, N 5.01; found C 63.25, H 7.52, N 5.35 %.

***n*-Octyl 4-aminobenzoate, 4.c.3**

Yield 88%, m. p. 69-70˚C. ν_{max}: 3417, 3330, 3219, 2922, 2852, 1683, 1637, 1595, 1172, 1120 cm^{-1}; δ_H: 7.85 (d, ^3J 8.64 Hz, 2H, Ar-H), 6.63 (d, ^3J 8.52 Hz, 2H, Ar-H), 4.24 (t, ^3J 6.64 Hz, 2H, Ar-COO-CH_2-), 4.03 (s, 2H, Ar-NH_2) 1.76-1.69 (quin, ^3J 6.64 Hz, 2H, Ar-COO-CH_2-$\underline{CH_2}$-), 1.42-1.27 (m, 10H, (-CH_2-)$_5$), 0.87 (t, ^3J 6.48 Hz, 3H, -CH_3); $C_{15}H_{23}NO_2$ requires C 72.25, H 9.29, N 5.62; found C 72.74, H 9.27, N 5.70 %.

***n*-Nonyl 4-nitrobenzoate, 4.b.4**

Yield 75%, viscous liquid. ν_{max}: 2954, 2925, 2854, 1728, 1726, 1724, 1608, 1529, 1467, 1274, 1014 cm^{-1}; δ_H: 8.26 (d, ^3J 8.92 Hz, 2H, Ar-H), 8.18 (d, ^3J 8.92 Hz, 2H, Ar-H), 4.35 (t, ^3J 6.72 Hz, 2H, Ar-COO-CH_2-), 1.81-1.74 (quin, ^3J 6.72 Hz, 2H, Ar-COO-CH_2-$\underline{CH_2}$-), 1.46-1.26 (m, 12H, (-CH_2-)$_6$), 0.85 (t, ^3J 6.5 Hz, 3H, -CH_3); $C_{16}H_{23}NO_4$ requires C 65.51, H 7.89, N 4.77; found C 65.35, H 7.55, N 5.11 %.

***n*-Nonyl 4-aminobenzoate, 4.c.4**

Yield 87%, m. p. 68-70˚C. ν_{max}: 3415, 3330, 3317, 3220, 2922, 2852, 1685, 1681, 1514, 1461, 1280, 1120 cm^{-1}; δ_H: 7.85 (d, ^3J 8.68 Hz, 2H, Ar-H), 6.63 (d, ^3J 8.68 Hz, 2H, Ar-H), 4.24 (t, ^3J

6.68 Hz, 2H, Ar-COO-CH_2-), 4.03 (s, 2H, Ar-NH_2) 1.76-1.69 (quin, ^3J 6.72 Hz, 2H, Ar-COO-CH_2-$\underline{CH_2}$-), 1.42-1.27 (m, 12H, $(-CH_2-)_6$), 0.87 (t, ^3J 6.56 Hz, 3H, -CH_3); $C_{16}H_{25}NO_2$ requires C 72.97, H 9.56, N 5.32; found C 72.66, H 9.36, N 5.18 %.

_n_-Decyl 4-nitrobenzoate, 4.b.5

Yield 82%, viscous liquid. ν_{max}: 2958, 2920, 2852, 1716, 1606, 1525, 1469, 1352, 1286, 1122, 1105 cm^{-1}; δ_H: 8.28 (d, ^3J 8.92 Hz, 2H, Ar-H), 8.20 (d, ^3J 8.92 Hz, 2H, Ar-H), 4.36 (t, ^3J 6.68 Hz, 2H, Ar-COO-CH_2-), 1.82-1.75 (quin, ^3J 6.72 Hz, 2H, Ar-COO-CH_2-$\underline{CH_2}$-), 1.47-1.26 (m, 14H, $(-CH_2-)_7$), 0.87 (t, ^3J 6.5 Hz, 3H, -CH_3); $C_{17}H_{25}NO_4$ requires C 66.43, H 8.1, N 4.55; found C 66.0, H 7.97, N 4.45 %.

_n_-Decyl 4-aminobenzoate, 4.c.5

Yield 89%, m. p. 75-76˚C. ν_{max}: 3417, 3330, 3220, 2920, 2852, 1685, 1683, 1637, 1595, 1514, 1465, 1379, 1311, 1280, 1172 cm^{-1}; δ_H: 7.85 (d, ^3J 8.64 Hz, 2H, Ar-H), 6.63 (d, ^3J 8.64 Hz, 2H, Ar-H), 4.24 (t, ^3J 6.64 Hz, 2H, Ar-COO-CH_2-), 4.03 (s, 2H, Ar-NH_2) 1.76-1.69 (quin, ^3J 6.76 Hz, 2H, Ar-COO-CH_2-$\underline{CH_2}$-), 1.42-1.27 (m, 14H, $(-CH_2-)_7$), 0.87 (t, ^3J 6.56 Hz, 3H, -CH_3); $C_{17}H_{27}NO_2$ requires C 73.6, H 9.8, N 5.0; found C 73.15, H 9.80, N 4.84 %.

_n_-Undecyl 4-nitrobenzoate, 4.b.6

Yield 79%, viscous liquid. ν_{max}: 2923, 2854, 1728, 1724, 1720, 1608, 1529, 1467, 1350, 1274, 1116, 1103, 1014 cm^{-1}; δ_H: 8.28 (d, ^3J 8.92 Hz, 2H, Ar-H), 8.20 (d, ^3J 8.92 Hz, 2H, Ar-H), 4.36 (t, ^3J 6.68 Hz, 2H, Ar-COO-CH_2-), 1.82-1.75 (quin, ^3J 6.76 Hz, 2H, Ar-COO-CH_2-$\underline{CH_2}$-), 1.47-1.26 (m, 16H, $(-CH_2-)_8$), 0.87 (t, ^3J 6.6 Hz, 3H, -CH_3); $C_{18}H_{27}NO_4$ requires C 67.27, H 8.45, N 4.36; found C 66.45, H 8.40, N 4.28 %.

_n_-Undecyl 4-aminobenzoate, 4.c.6

Yield 90%, m. p. 76-78˚C. ν_{max}: 3413, 3330, 3317, 3220, 2922, 2848, 1683, 1639, 1596, 1573, 1514, 1463, 1444, 1380, 1311, 1282, 1172, 1120 cm^{-1}; δ_H: 7.85 (d, ^3J 8.72 Hz, 2H, Ar-H), 6.63 (d, ^3J 8.72 Hz, 2H, Ar-H), 4.24 (t, ^3J 6.68 Hz, 2H, Ar-COO-CH_2-), 4.03 (s, 2H, Ar-NH_2) 1.76-1.69 (quin, ^3J 6.60 Hz, 2H, Ar-COO-CH_2-$\underline{CH_2}$-), 1.43-1.26 (m, 16H, $(-CH_2-)_8$), 0.87 (t, ^3J 6.6 Hz, 3H, -CH_3); $C_{18}H_{29}NO_2$ requires C 74.19, H 10.02, N 4.80; found C 73.69, H 10.0, N 4.49 %.

***n*-Dodecyl 4-nitrobenzoate, 4.b.7**

Yield 82%, m. p. 41-42.5˚C. ν_{max}: 2920, 2850, 1716, 1714, 1606, 1527, 1469, 1465, 1458, 1377, 1352, 1290, 1124 cm^{-1}; δ_H: 8.28 (d, ^3J 8.92 Hz, 2H, Ar-H), 8.20 (d, ^3J 8.92 Hz, 2H, Ar-H), 4.36 (t, ^3J 6.68 Hz, 2H, Ar-COO-CH_2-), 1.82-1.75 (quin, ^3J 6.76 Hz, 2H, Ar-COO-CH_2-$\underline{CH_2}$-), 1.47-1.26 (m, 18H, (-CH_2-)$_9$), 0.87 (t, ^3J 6.6 Hz, 3H, -CH_3); $C_{19}H_{29}NO_4$ requires C 68.03, H 8.71, N 4.17; found C 67.66, H 8.82, N 3.83 %.

***n*-Dodecyl 4-aminobenzoate, 4.c.7**

Yield 88%, m. p. 77-78˚C. ν_{max}: 3415, 3332, 3220, 2920, 2850, 1687, 1685, 1596, 1458, 1284, 1172, 1122 cm^{-1}; δ_H: 7.85 (d, ^3J 8.72 Hz, 2H, Ar-H), 6.63 (d, ^3J 8.72 Hz, 2H, Ar-H), 4.24 (t, ^3J 6.68 Hz, 2H, Ar-COO-CH_2-), 4.03 (s, 2H, Ar-NH_2) 1.76-1.69 (quin, ^3J 6.68 Hz, 2H, Ar-COO-CH_2-$\underline{CH_2}$-), 1.42-1.26 (m, 18H, (-CH_2-)$_9$), 0.87 (t, ^3J 6.6 Hz, 3H, -CH_3); $C_{19}H_{31}NO_2$ requires C 74.72, H 10.22, N 4.58; found C 74.57, H 10.20, N 4.34 %.

***n*-Tridecyl 4-nitrobenzoate, 4.b.8**

Yield 75%, m. p. 37-38˚C. ν_{max}: 2920, 2850, 1712, 1714, 1604, 1525, 1469, 1377, 1350, 1288, 1122 cm^{-1}; δ_H: 8.28 (d, ^3J 8.92 Hz, 2H, Ar-H), 8.20 (d, ^3J 8.92 Hz, 2H, Ar-H), 4.36 (t, ^3J 6.68 Hz, 2H, Ar-COO-CH_2-), 1.82-1.75 (quin, ^3J 6.76 Hz, 2H, Ar-COO-CH_2-$\underline{CH_2}$-), 1.47-1.26 (m, 20H, (-CH_2-)$_{10}$), 0.87 (t, ^3J 6.6 Hz, 3H, -CH_3); $C_{20}H_{31}NO_4$ requires C 68.75, H 8.93, N 4.50; found C 68.26, H 8.54, N 4.18 %.

***n*-Tridecyl 4-aminobenzoate, 4.c.8**

Yield 85%, m. p. 84-85˚C. ν_{max}: 3415, 3413, 3332, 3220, 2920, 2850, 1687, 1685, 1596, 1460, 1282, 1172, 1120 cm^{-1}; δ_H: 7.85 (d, ^3J 8.72 Hz, 2H, Ar-H), 6.63 (d, ^3J 8.72 Hz, 2H, Ar-H), 4.24 (t, ^3J 6.68 Hz, 2H, Ar-COO-CH_2-), 4.03 (s, 2H, Ar-NH_2) 1.76-1.69 (quin, ^3J 6.68 Hz, 2H, Ar-COO-CH_2-$\underline{CH_2}$-), 1.42-1.26 (m, 20H, (-CH_2-)$_{10}$), 0.87 (t, ^3J 6.6 Hz, 3H, -CH_3); $C_{20}H_{33}NO_2$ requires C 75.20, H 10.40, N 4.38; found C 74.85, H 10.12, N 3.92 %.

***n*-Tetradecyl 4-nitrobenzoate, 4.b.9**

Yield 75%, m. p. 50.5-51.5˚C. ν_{max}: 2920, 2850, 1712, 1695, 1479, 1469, 1377, 1284, 1298, 1203, 1124, 1103 cm^{-1}; δ_H: 8.28 (d, ^3J 8.92 Hz, 2H, Ar-H), 8.20 (d, ^3J 8.92 Hz, 2H, Ar-H), 4.36 (t, ^3J

6.68 Hz, 2H, Ar-COO-CH_2-), 1.82-1.75 (quin, ^3J 6.76 Hz, 2H, Ar-COO-CH_2-$\underline{CH_2}$-), 1.47-1.26 (m, 22H, $(-CH_2-)_{11}$), 0.87 (t, ^3J 6.6 Hz, 3H, -CH_3); $C_{21}H_{33}NO_4$ requires C 69.39, H 9.15, N 3.85; found C 69.08, H 9.14, N 3.60 %.

***n*-Tetradecyl 4-aminobenzoate, 4.c.9**

Yield 89%, m. p. 92-93˚C. ν_{max}: 3415, 3332, 3220, 2920, 2850, 1685, 1683, 1637, 1595, 1514, 1465, 1380, 1311, 1284, 1172, 1120 cm^{-1}; δ_H: 7.85 (d, ^3J 8.60 Hz, 2H, Ar-H), 6.63 (d, ^3J 8.60 Hz, 2H, Ar-H), 4.25 (t, ^3J 6.64 Hz, 2H, Ar-COO-CH_2-), 4.03 (s, 2H, Ar-NH_2) 1.76-1.69 (quin, ^3J 6.68 Hz, 2H, Ar-COO-CH_2-$\underline{CH_2}$-), 1.42-1.26 (m, 22H, $(-CH_2-)_{11}$), 0.87 (t, ^3J 6.6 Hz, 3H, -CH_3); $C_{21}H_{35}NO_2$ requires C 75.62, H 10.57, N 4.19; found C 75.66, H 10.56, N 3.86 %.

***n*-Hexadecyl 4-nitrobenzoate, 4.b.10**

Yield 78%, m. p. 58-59˚C. ν_{max}: 2922, 2850, 1716, 1714, 1606, 1525, 1469, 1352, 1288, 1124, 1105 cm^{-1}; δ_H: 8.28 (d, ^3J 8.92 Hz, 2H, Ar-H), 8.20 (d, ^3J 8.92 Hz, 2H, Ar-H), 4.36 (t, ^3J 6.68 Hz, 2H, Ar-COO-CH_2-), 1.82-1.75 (quin, ^3J 6.76 Hz, 2H, Ar-COO-CH_2-$\underline{CH_2}$-), 1.47-1.26 (m, 26H, $(-CH_2-)_{13}$), 0.87 (t, ^3J 6.6 Hz, 3H, -CH_3); $C_{23}H_{37}NO_4$ requires C 70.56, H 9.52, N 3.58; found C 70.90, H 9.39, N 3.43 %.

***n*-Hexadecyl 4-aminobenzoate, 4.c.10**

Yield 90%, m. p. 88-89.5˚C. ν_{max}: 3415, 3330, 3219, 2922, 2852, 1685, 1683, 1637, 1596, 1514, 1463, 1377, 1311, 1282, 1172, 1120 cm^{-1}; δ_H: 7.85 (d, ^3J 8.60 Hz, 2H, Ar-H), 6.63 (d, ^3J 8.60 Hz, 2H, Ar-H), 4.25 (t, ^3J 6.64 Hz, 2H, Ar-COO-CH_2-), 4.03 (s, 2H, Ar-NH_2) 1.76-1.69 (quin, ^3J 6.64 Hz, 2H, Ar-COO-CH_2-$\underline{CH_2}$-), 1.42-1.26 (m, 26H, $(-CH_2-)_{13}$), 0.87 (t, ^3J 6.6 Hz, 3H, -CH_3); $C_{23}H_{39}NO_2$ requires C 76.4, H 10.87, N 3.87; found C 76.79, H 10.52, N 3.72 %.

***n*-Octadecyl 4-nitrobenzoate, 4.b.11**

Yield 80%, m. p. 63-64˚C. ν_{max}: 2922, 2850, 1716, 1714, 1606, 1525, 1469, 1460, 1352, 1290, 1124, 1105 cm^{-1}; δ_H: 8.28 (d, ^3J 8.92 Hz, 2H, Ar-H), 8.20 (d, ^3J 8.92 Hz, 2H, Ar-H), 4.36 (t, ^3J 6.72 Hz, 2H, Ar-COO-CH_2-), 1.82-1.75 (quin, ^3J 6.76 Hz, 2H, Ar-COO-CH_2-$\underline{CH_2}$-), 1.47-1.26 (m, 30H, $(-CH_2-)_{15}$), 0.87 (t, ^3J 6.6 Hz, 3H, -CH_3); $C_{25}H_{41}NO_4$ requires C 71.56, H 9.85, N 3.34; found C 71.29, H 9.4, N 2.90 %.

_n_-Octadecyl 4-aminobenzoate, 4.c.11

Yield 89%, m. p. 93-94˚C. ν_{max}: 3415, 3330, 3220, 2922, 2852, 1687, 1685, 1639, 1596, 1514, 1461, 1284, 1172, 1122 cm^{-1}; δ_H: 7.85 (d, ^3J 8.60 Hz, 2H, Ar-H), 6.63 (d, ^3J 8.60 Hz, 2H, Ar-H), 4.25 (t, ^3J 6.68 Hz, 2H, Ar-COO-CH_2-), 4.03 (s, 2H, Ar-NH_2) 1.76-1.69 (quin, ^3J 6.76 Hz, 2H, Ar-COO-CH_2-$\underline{CH_2}$-), 1.42-1.26 (m, 30H, $(-CH_2-)_{15}$), 0.87 (t, ^3J 6.6 Hz, 3H, -CH_3); $C_{25}H_{43}NO_2$ requires C 77.0, H 11.12, N 3.5; found C 76.52, H 10.93, N 3.38 %.

4-(4-_n_-Hexyloxycarbonylphenyliminomethyl)benzoic acid, 4.d.1

A mixture of compound **4.c.1** (2g, 6.8 mmol), 4-formylbenzoic acid, **4.ii** (1.0g, 6.8 mmol) and a few drops of acetic acid in toluene (25 ml) was refluxed for 5 hours using a Dean-Stark apparatus. The reaction mixture was cooled to room temperature and the crystallized product was filtered and dried. Yield 2.5g (89%), Cr 146.0 SmX 163.0 SmC 226.5 SmA 240.5 I. ν_{max}: 3070, 2956, 2927, 2856, 2667, 2549, 1708, 1678, 1672, 1787, 1625, 1608, 1593, 1568, 1427, 1274, 1166, 1105 cm^{-1}; δ_H: 8.52 (s, 1H, -CH═N-), 8.23 (d, ^3J 8.3 Hz, 2H, Ar-H), 8.09 (d, ^3J 8.5 Hz, 2H, Ar-H), 8.02 (d, ^3J 8.3 Hz, 2H, Ar-H), 7.24 (*d*, ^3J 8.52 Hz, 2H, Ar-H), 4.33 (t, ^3J 6.68 Hz, 2H, Ar-COO-CH_2-), 1.80-1.75 (quin, ^3J 6.68 Hz, 2H, Ar-COO-CH_2-$\underline{CH_2}$-), 1.45-1.27 (m, 6H, $(-CH_2-)_3$), 0.91 (t, ^3J 6.9 Hz, 3H, -CH_3); $C_{21}H_{23}NO_4$ requires C 71.38, H 6.55, N 3.96; found C 71.81, H 6.23, N 3.96 %.

4-(4-_n_-Heptyloxycarbonylphenyliminomethyl)benzoic acid, 4.d.2

Yield 85%, m. p. 126.0˚C. ν_{max}: 3016, 2929, 2852, 2661, 2592, 2540, 1942, 1679, 1666, 1643, 1608, 1566, 1413, 1386, 1361, 1164, 1190, 1103, 1016 cm^{-1}; δ_H: 8.52 (s, 1H, -CH═N-), 8.23 (d, ^3J 8.3 Hz, 2H, Ar-H), 8.10 (d, ^3J 8.44 Hz, 2H, Ar-H), 8.03 (d, ^3J 8.3 Hz, 2H, Ar-H), 7.24 (*d*, ^3J 8.42 Hz, 2H, Ar-H), 4.33 (t, ^3J 6.64 Hz, 2H, Ar-COO-CH_2-), 1.80-1.75 (quin, ^3J 6.72 Hz, 2H, Ar-COO-CH_2-$\underline{CH_2}$-), 1.48-1.31 (m, 8H, $(-CH_2-)_4$), 0.89 (t, ^3J 6.5 Hz, 3H, -CH_3); $C_{22}H_{25}NO_4$ requires C 71.91, H 6.85, N 3.81; found C 71.52, H 6.74, N 3.60 %.

4-(4-_n_-Octyloxycarbonylphenyliminomethyl)benzoic acid, 4.d.3

Yield 83%, m. p. 112.5˚C. ν_{max}: 3058, 2920, 2850, 2667, 2542, 1942, 1712, 1703, 1687, 1681, 1595, 1569, 1469, 1429, 1413, 1278, 1168, 1116 cm^{-1}; δ_H: 8.52 (s, 1H, -CH═N-), 8.23 (d, ^3J 8.3 Hz, 2H, Ar-H), 8.10 (d, ^3J 8.44 Hz, 2H, Ar-H), 8.03 (d, ^3J 8.3 Hz, 2H, Ar-H), 7.24 (*d*, ^3J 8.42 Hz,

2H, Ar-H), 4.33 (t, ^{3}J 6.64 Hz, 2H, Ar-COO-CH_2-), 1.80-1.75 (quin, ^{3}J 6.72 Hz, 2H, Ar-COO-CH_2-$\underline{CH_2}$-), 1.48-1.31 (m, 10H, (-CH_2-)$_5$), 0.89 (t, ^{3}J 6.5 Hz, 3H, -CH_3); $C_{23}H_{27}NO_4$ requires C 72.42, H 7.13, N 3.67; found C 72.84, H 6.85, N 3.38 %.

4-(4-*n*-Nonyloxycarbonylphenyliminomethyl)benzoic acid, 4.d.4

Yield 87%, m. p. 109.5˚C. ν_{max}: 3051, 2958, 2920, 2850, 2667, 2543, 1942, 1712, 1710, 1685, 1681, 1595, 1569, 1429, 1413, 1276, 1168, 1116, 1012 cm^{-1}; δ_H: 8.52 (s, 1H, -CH═N-), 8.23 (d, ^{3}J 8.3 Hz, 2H, Ar-H), 8.10 (d, ^{3}J 8.44 Hz, 2H, Ar-H), 8.03 (d, ^{3}J 8.3 Hz, 2H, Ar-H), 7.24 (*d*, ^{3}J 8.42 Hz, 2H, Ar-H), 4.33 (t, ^{3}J 6.64 Hz, 2H, Ar-COO-CH_2-), 1.80-1.75 (quin, ^{3}J 6.72 Hz, 2H, Ar-COO-CH_2-$\underline{CH_2}$-), 1.48-1.28 (m, 12H, (-CH_2-)$_6$), 0.89 (t, ^{3}J 6.5 Hz, 3H, -CH_3); $C_{24}H_{29}NO_4$ requires C 72.89, H 7.38, N 3.54; found C 72.57, H 7.37, N 3.44 %.

4-(4-*n*-Decyloxycarbonylphenyliminomethyl)benzoic acid, 4.d.5

Yield 89%, m. p. 116.0˚C. ν_{max}: 3062, 2958, 2918, 2848, 2752, 2671, 2557, 2086, 1969, 1924, 1735, 1733, 1710, 1695, 1685, 1016 cm^{-1}; δ_H: 8.52 (s, 1H, -CH═N-), 8.23 (d, ^{3}J 8.3 Hz, 2H, Ar-H), 8.10 (d, ^{3}J 8.52 Hz, 2H, Ar-H), 8.03 (d, ^{3}J 8.3 Hz, 2H, Ar-H), 7.24 (*d*, ^{3}J 8.52 Hz, 2H, Ar-H), 4.33 (t, ^{3}J 6.64 Hz, 2H, Ar-COO-CH_2-), 1.80-1.75 (quin, ^{3}J 6.68 Hz, 2H, Ar-COO-CH_2-$\underline{CH_2}$-), 1.45-1.28 (m, 14H, (-CH_2-)$_7$), 0.89 (t, ^{3}J 6.5 Hz, 3H, -CH_3); $C_{25}H_{31}NO_4$ requires C 73.32, H 7.62, N 3.42; found C 72.97, H 7.58, N 3.17 %.

4-(4-*n*-Undecyloxycarbonylphenyliminomethyl)benzoic acid, 4.d.6

Yield 85%, m. p. 115.0˚C. ν_{max}: 3057, 2958, 2918, 2848, 2667, 2542, 1712, 1710, 1685, 1681, 1595, 1569, 1469, 1429, 1413, 1278, 1168, 1118 1012 cm^{-1}; δ_H: 8.52 (s, 1H, -CH═N-), 8.23 (d, ^{3}J 8.3 Hz, 2H, Ar-H), 8.10 (d, ^{3}J 8.52 Hz, 2H, Ar-H), 8.03 (d, ^{3}J 8.3 Hz, 2H, Ar-H), 7.24 (*d*, ^{3}J 8.52 Hz, 2H, Ar-H), 4.33 (t, ^{3}J 6.64 Hz, 2H, Ar-COO-CH_2-), 1.80-1.75 (quin, ^{3}J 6.68 Hz, 2H, Ar-COO-CH_2-$\underline{CH_2}$-), 1.45-1.28 (m, 16H, (-CH_2-)$_8$), 0.89 (t, ^{3}J 6.5 Hz, 3H, -CH_3); $C_{26}H_{33}NO_4$ requires C 73.73, H 7.85, N 3.31; found C 73.23, H 7.73, N 3.07 %.

4-(4-*n*-Dodecyloxycarbonylphenyliminomethyl)benzoic acid, 4.d.7

Yield 87%, m. p. 120.0˚C. ν_{max}: 3058, 2954, 2918, 2848, 2667, 2542, 1940, 1712, 1685, 1681, 1595, 1569, 1471, 1429, 1415, 1361, 1278, 1170, 1122 cm^{-1}; δ_H: 8.52 (s, 1H, -CH═N-), 8.23 (d, ^{3}J

8.2 Hz, 2H, Ar-H), 8.10 (d, ^{3}J 8.52 Hz, 2H, Ar-H), 8.03 (d, ^{3}J 8.2 Hz, 2H, Ar-H), 7.24 (*d*, ^{3}J 8.52 Hz, 2H, Ar-H), 4.33 (t, ^{3}J 6.64 Hz, 2H, Ar-COO-CH_2-), 1.80-1.75 (quin, ^{3}J 6.68 Hz, 2H, Ar-COO-CH_2-$\underline{CH_2}$-), 1.45-1.28 (m, 18H, (-CH_2-)$_9$), 0.89 (t, ^{3}J 6.5 Hz, 3H, -CH_3); $C_{27}H_{35}NO_4$ requires C 74.11, H 8.06, N 3.20; found C 74.35, H 7.81, N 2.91 %.

4-(4-*n*-Tridecyloxycarbonylphenyliminomethyl)benzoic acid, 4.d.8

Yield 88%, m. p. 119.0˚C. ν_{max}: 3057, 2920, 2850, 2669, 2547, 1712, 1699, 1685, 1683, 1595, 1569, 1465, 1431, 1280, 1126 cm^{-1}; δ_H: 8.52 (s, 1H, -CH═N-), 8.23 (d, ^{3}J 8.2 Hz, 2H, Ar-H), 8.10 (d, ^{3}J 8.52 Hz, 2H, Ar-H), 8.03 (d, ^{3}J 8.2 Hz, 2H, Ar-H), 7.24 (*d*, ^{3}J 8.52 Hz, 2H, Ar-H), 4.33 (t, ^{3}J 6.64 Hz, 2H, Ar-COO-CH_2-), 1.80-1.75 (quin, ^{3}J 6.68 Hz, 2H, Ar-COO-CH_2-$\underline{CH_2}$-), 1.45-1.28 (m, 20H, (-CH_2-)$_{10}$), 0.89 (t, ^{3}J 6.5 Hz, 3H, -CH_3); $C_{28}H_{37}NO_4$ requires C 74.47, H 8.26, N 3.1; found C 74.0, H 8.35, N 3.2 %.

4-(4-*n*-Tetradecyloxycarbonylphenyliminomethyl)benzoic acid, 4.d.9

Yield 84%, m. p. 123.5˚C. ν_{max}: 3057, 2920, 2850, 2669, 2547, 1712, 1669, 1685, 1683, 1595, 1569, 1465, 1431, 1415, 1280, 1126 cm^{-1}; δ_H: 8.52 (s, 1H, -CH═N-), 8.23 (d, ^{3}J 8.2 Hz, 2H, Ar-H), 8.10 (d, ^{3}J 8.52 Hz, 2H, Ar-H), 8.03 (d, ^{3}J 8.2 Hz, 2H, Ar-H), 7.24 (*d*, ^{3}J 8.52 Hz, 2H, Ar-H), 4.33 (t, ^{3}J 6.64 Hz, 2H, Ar-COO-CH_2-), 1.80-1.75 (quin, ^{3}J 6.68 Hz, 2H, Ar-COO-CH_2-$\underline{CH_2}$-), 1.45-1.28 (m, 22H, (-CH_2-)$_{11}$), 0.89 (t, ^{3}J 6.5 Hz, 3H, -CH_3); $C_{29}H_{39}NO_4$ requires C 74.8, H 8.40, N 3.0; found C 74.54, H 8.34, N 2.71 %.

4-(4-*n*-Hexadecyloxycarbonylphenyliminomethyl)benzoic acid, 4.d.10

Yield 87%, m. p. 125.0˚C. ν_{max}: 2920, 2850, 2671, 2549, 1712, 1687, 1683, 1612, 1595, 1463, 1377, 1278 cm^{-1}; δ_H: 8.52 (s, 1H, -CH═N-), 8.23 (d, ^{3}J 8.2 Hz, 2H, Ar-H), 8.10 (d, ^{3}J 8.52 Hz, 2H, Ar-H), 8.03 (d, ^{3}J 8.2 Hz, 2H, Ar-H), 7.24 (*d*, ^{3}J 8.52 Hz, 2H, Ar-H), 4.33 (t, ^{3}J 6.64 Hz, 2H, Ar-COO-CH_2-), 1.80-1.75 (quin, ^{3}J 6.68 Hz, 2H, Ar-COO-CH_2-$\underline{CH_2}$-), 1.45-1.28 (m, 26H, (-CH_2-)$_{13}$), 0.89 (t, ^{3}J 6.5 Hz, 3H, -CH_3); $C_{31}H_{43}NO_4$ requires C 75.4, H 8.70, N 2.80; found C 75.84, H 8.65, N 2.55 %.

4-(4-*n*-Octadecyloxycarbonylphenyliminomethyl)benzoic acid, 4.d.11

Yield 86%, m. p. 126.5˚C. ν_{max}: 2920, 2850, 2617, 2549, 1712, 1710, 1687, 1685, 1463, 1280

cm^{-1}; δ_H: 8.52 (s, 1H, -CH═N-), 8.23 (d, ^3J 8.2 Hz, 2H, Ar-H), 8.10 (d, ^3J 8.52 Hz, 2H, Ar-H), 8.03 (d, ^3J 8.2 Hz, 2H, Ar-H), 7.24 (*d*, ^3J 8.52 Hz, 2H, Ar-H), 4.33 (t, ^3J 6.64 Hz, 2H, Ar-COO-CH_2-), 1.80-1.75 (quin, ^3J 6.68 Hz, 2H, Ar-COO-CH_2-$\underline{CH_2}$-), 1.45-1.28 (m, 30H, $(-CH_2-)_{15}$), 0.89 (t, ^3J 6.5 Hz, 3H, $-CH_3$); $C_{33}H_{47}NO_4$ requires C 75.9, H 9.08, N 2.68; found C 76.27, H 8.81, N 2.36 %.

_n_-Decyl 4-formylbenzoate, 4.g.1

A mixture of 4-formylbenzoic acid, **4.e** (2g, 13.3 mmol), *n*-decanol, **4.f** (2.1g, 13.3 mmol) in dry dichloromethane (25 ml) and a catalytic amount of DMAP was stirred for 15 minutes. To this stirred mixture, DCC (3.0g, 14.6 mmol) was added and stirring continued for 4 hours at room temperature. The precipitated *N*, *N*′–dicyclohexylurea was filtered off and washed thoroughly with chloroform. The solvent from the filtrate was evaporated to obtain a residue, which was chromatographed on silica gel using a mixture of chloroform and hexane in the ratio 2:3 as an eluant. Removal of solvent from the eluate provided the required product. Yield 3g (79%), viscous liquid. ν_{max}: 2922, 2852, 2729, 1724, 1714, 1695, 1460, 1284 cm^{-1}; δ_H: 10.1 (s, 1H, Ar-CHO), 8.19 (d, ^3J 8.2 Hz, 2H, Ar-H), 7.94 (d, ^3J 8.3 Hz, 2H, Ar-H), 4.35 (t, ^3J 6.7 Hz, 2H, Ar-COO-CH_2-), 1.82-1.75 (quin, ^3J 6.76 Hz, 2H, Ar-COO-CH_2-C$\underline{H_2}$-), 1.55-1.34 (m, 14H, $(-CH_2-)_7$), 0.88 (t, ^3J 6.7 Hz, 3H, $-CH_3$); $C_{18}H_{26}O_3$ requires C 74.45, H 9.02; found C 74.0, H 8.85 %.

_n_-Undecyl 4-formylbenzoate, 4.g.2

Yield 75%, viscous liquid. ν_{max}: 2923, 2852, 2729, 1718, 1577, 1465, 1382, 1274 cm^{-1}; δ_H: 10.1 (s, 1H, Ar-CHO), 8.19 (d, ^3J 8.2. Hz, 2H, Ar-H), 7.94 (d, ^3J 8.3 Hz, 2H, Ar-H), 4.35 (t, ^3J 6.7 Hz, 2H, Ar-COO-CH_2-), 1.82-1.75 (quin, ^3J 6.76 Hz, 2H, Ar-COO-CH_2-C$\underline{H_2}$-), 1.55-1.34 (m, 16H, $(-CH_2-)_8$), 0.88 (t, ^3J 6.7 Hz, 3H, $-CH_3$); $C_{19}H_{28}O_3$ requires C 74.96, H 9.27; found C 74.65, H 9.28 %.

_n_-Dodecyl 4-formylbenzoate, 4.g.3

Yield 78%, viscous liquid. ν_{max}: 2923, 2852, 2729, 1724, 1718, 1708, 1577, 1465, 1382, 1274 cm^{-1}; δ_H: 10.1 (s, 1H, Ar-CHO), 8.19 (d, ^3J 8.2 Hz, 2H, Ar-H), 7.94 (d, ^3J 8.3 Hz, 2H, Ar-H), 4.35 (t, ^3J 6.7 Hz, 2H, Ar-COO-CH_2-), 1.82-1.75 (quin, ^3J 6.76 Hz, 2H, Ar-COO-CH_2-C$\underline{H_2}$-), 1.55-1.34 (m, 18H, $(-CH_2-)_9$), 0.88 (t, ^3J 6.7 Hz, 3H, $-CH_3$); $C_{20}H_{30}O_3$ requires C 75.43, H 9.49; found

C 75.8, H 9.0 %.

_n_-Tetradecyl 4-formylbenzoate, 4.g.4

Yield 78%, m. p. 39-40˚C. ν_{max}: 2923, 2852, 2729, 1714, 1695, 1460, 1377, 1284 cm^{-1}; δ_H: 10.1 (s, 1H, Ar-CHO), 8.19 (d, ^3J 8.2 Hz, 2H, Ar-H), 7.94 (d, ^3J 8.3 Hz, 2H, Ar-H), 4.35 (t, ^3J 6.7 Hz, 2H, Ar-COO-CH_2-), 1.82-1.75 (quin, ^3J 6.76 Hz, 2H, Ar-COO-CH_2-C$\underline{H_2}$-), 1.55-1.34 (m, 22H, (-CH_2-)$_{11}$), 0.88 (t, ^3J 6.7 Hz, 3H, -CH_3); $C_{22}H_{34}O_3$ requires C 76.23, H 9.89; found C 75.78, H 9.72 %.

_n_-Hexadecyl 4-formylbenzoate, 4.g.5

Yield 80%, m. p. 49-50˚C. ν_{max}: 2952, 2923, 2852, 2729, 1716, 1695, 1469, 1377, 1286 cm^{-1}; δ_H: 10.1 (s, 1H, Ar-CHO), 8.19 (d, ^3J 8.2 Hz, 2H, Ar-H), 7.94 (d, ^3J 8.3 Hz, 2H, Ar-H), 4.35 (t, ^3J 6.7 Hz, 2H, Ar-COO-CH_2-), 1.82-1.75 (quin, ^3J 6.76 Hz, 2H, Ar-COO-CH_2-C$\underline{H_2}$-), 1.55-1.34 (m, 26H, (-CH_2-)$_{13}$), 0.88 (t, ^3J 6.7 Hz, 3H, -CH_3); Elemental analysis: $C_{24}H_{38}O_3$ requires C 76.96, H 10.02; found C 76.52, H 10.27 %.

_n_-Octadecyl 4-formylbenzoate, 4.g.6

Yield 78%, m. p. 55-56˚C. ν_{max}: 2952, 2923, 2852, 2729, 1716, 1695, 1469, 1377, 1286 cm^{-1}; δ_H: 10.1 (s, Ar-CHO), 8.19 (d, ^3J 8.2 Hz, 2H, Ar-H), 7.94 (d, ^3J 8.3 Hz, 2H, Ar-H), 4.35 (t, ^3J 6.7 Hz, 2H, Ar-COO-CH_2-), 1.82-1.75 (quin, ^3J 6.76, 2H, Ar-COO-CH_2-C$\underline{H_2}$-), 1.55-1.34 (m, 30H, (-CH_2-)$_{15}$), 0.88 (t, ^3J 6.7Hz, 3H, -CH_3); Elemental analysis: $C_{26}H_{42}O_3$ requires C 77.58, H 10.50; found C 77.98, H 10.47 %.

4-(4-_n_-Decyloxycarbonylbenzylideneamino)benzoic acid, 4.h.1

A mixture of *n*-decyl 4-formylbenzoate, **4.g.1** (1.8g, 6.2 mmol), 4-aminobenzoic acid, **4.iv** (0.85g, 6.2 mmol) and a few drops of acetic acid in dry toluene (20 ml) was refluxed using a Dean-Stark apparatus for 4 hours. The solution was cooled to room temperature and the precipitated product was filtered off. The product was crystallized again from toluene. Yield: 2.2g (88%), Cr 133.5 SmX 164.0 SmC 234.5 I. ν_{max}: 2952, 2922, 2850, 2673, 2553, 1934, 1693, 1679, 1608, 1569, 1465, 1429, 1282, 1112 cm^{-1}; δ_H: 8.5 (s, 1H, -CH=N-), 8.17-8.15 (m, 4H, Ar-H), 7.99 (d, ^3J 7.52

Hz, 2H, Ar-H), 7.26 (d, ^3J 6 Hz, 2H, Ar-H), 4.34 (t, ^3J 6.16 Hz, 2H, Ar-COO-CH_2-), 1.79-1.45 (m, 16H, (-CH_2-)$_8$), 0.86 (t, ^3J 6.52 Hz, 3H, -CH_3); Elemental analysis: $C_{25}H_{31}NO_4$ requires C 73.3, H 7.63, N 3.1; found C 72.9, H 8.03, N 3.0 %.

4-(4-*n*-Undecyloxycarbonylbenzylideneamino)benzoic acid, 4.h.2

Yield 80%, m. p. 131.0˚C. ν_{max}: 2952, 2922, 2850, 2673, 2553, 1934, 1693, 1679, 1608, 1569, 1465, 1429, 1282, 1112 cm^{-1}; δ_H: 8.5 (s, 1H, -CH═N-), 8.17-8.15 (m, 4H, Ar-H), 7.99 (d, ^3J 7.52 Hz, 2H, Ar-H), 7.26 (d, ^3J 6 Hz, 2H, Ar-H), 4.34 (t, ^3J 6.16 Hz, 2H, Ar-COOCH_2-), 1.79-1.45 (m, 18H, (-CH_2-)$_9$), 0.86 (t, ^3J 6.52 Hz, 3H, -CH_3); Elemental analysis: $C_{26}H_{33}NO_4$ requires C 73.73, H 7.85, N 3.3; found C 73.34, H 8.16, N 3.25 %.

4-(4-*n*-Dodecyloxycarbonylbenzylideneamino)benzoic acid, 4.h.3

Yield 85%, m. p. 130.5˚C. ν_{max}: 2952, 2922, 2850, 2673, 2553, 1934, 1693, 1679, 1608, 1569, 1465, 1429, 1282, 1112 cm^{-1}; δ_H: 8.5 (s, 1H, -CH═N-), 8.17-8.15 (m, 4H, Ar-H), 7.99 (d, ^3J 7.52 Hz, 2H, Ar-H), 7.26 (d, ^3J 6 Hz, 2H, Ar-H), 4.34 (t, ^3J 6.16 Hz, 2H, Ar-COO-CH_2-), 1.79-1.45 (m, 20H, (-CH_2-)$_{10}$), 0.86 (t, ^3J 6.52 Hz, 3H, -CH_3); Elemental analysis: $C_{27}H_{35}NO_4$ requires C 74.11, H 8.05, N 3.2; found C 74.34, H 8.26, N 3.15 %.

4-(4-*n*-Tetradecyloxycarbonylbenzylideneamino)benzoic acid, 4.h.4

Yield 82%, m. p. 130.0˚C. ν_{max}: 2918, 2848, 2669, 2553, 1708, 1681, 1596, 1569, 1429, 1278 cm^{-1}; δ_H: 8.5 (s, 1H, -CH═N-), 8.17-8.15 (m, 4H, Ar-H), 7.99 (d, ^3J 7.52 Hz, 2H, Ar-H), 7.26 (d, ^3J 6 Hz, 2H, Ar-H), 4.34 (t, ^3J 6.16 Hz, 2H, Ar-COO-CH_2-), 1.79-1.45 (m, 24H, (-CH_2-)$_{12}$), 0.86 (t, ^3J 6.52 Hz, 3H, -CH_3); Elemental analysis: $C_{29}H_{39}NO_4$ requires C 74.8, H 8.4, N 3.0; found C 74.46, H 8.32, N 3.05 %.

4-(4-*n*-Hexadecyloxycarbonylbenzylideneamino)benzoic acid, 4.h.5

Yield 86%, m. p. 130.5˚C. ν_{max}: 2952, 2918, 2848, 2675, 2555, 1708, 1693, 1687, 1681, 1596, 1429, 1282, 1118 cm^{-1}; δ_H: 8.5 (s, 1H, -CH═N-), 8.17-8.15 (m, 4H, Ar-H), 7.99 (d, ^3J 7.52 Hz, 2H, Ar-H), 7.26 (d, ^3J 6 Hz, 2H, Ar-H), 4.34 (t, ^3J 6.16 Hz, 2H, Ar-COO-CH_2-), 1.79-1.45 (m, 28H, (-CH_2-)$_{14}$), 0.86 (t, ^3J 6.52 Hz, 3H, -CH_3); Elemental analysis: $C_{31}H_{43}NO_4$ requires C 75.4, H 8.7, N 2.84; found C 75.26, H 8.68, N 2.51 %.

4-(4-*n*-Octadecyloxycarbonylbenzylideneamino)benzoic acid, 4.h.6

Yield 83%, m. p. 130.0˚C. ν_{max}: 2952, 2918, 2848, 2675, 2555, 1708, 1693, 1687, 1681, 1596, 1429, 1278, 1118 cm^{-1}; δ_H: 8.5 (s, 1H, -CH═N-), 8.17-8.15 (m, 4H, Ar-H), 7.99 (d, ^3J 7.52 Hz, 2H, Ar-H), 7.26 (d, ^3J 6 Hz, 2H, Ar-H), 4.34 (t, ^3J 6.16 Hz, 2H, Ar-COO-CH_2-), 1.79-1.45 (m, 32H, (-CH_2-)$_{16}$), 0.86 (t, ^3J 6.52 Hz, 3H, -CH_3); Elemental analysis: $C_{33}H_{47}NO_4$ requires C 75.9, H 9.08, N 2.68; found C 75.66, H 8.99, N 2.39 %.

1, 3-Phenylene bis [4-(4-*n*-hexyloxycarbonylphenyliminomethyl)benzoate], 4.A.1

A mixture of 1,3-dihydroxybenzene, **4.iii** (0.05g, 0.45 mmol), 4-(4-*n*-dodecyloxycarbonyl phenyliminomethyl)benzoic acid, **4.d.1** (0.32g, 0.9 mmol) and a catalytic amount of DMAP in dichloromethane (20 ml) was stirred for 15 minutes at room temperature. To this stirred mixture, DCC (0.2g, 1.0 mmol) was added and stirring continued for a further12 hours. The precipitated *N, N´*-dicyclohexylurea was filtered off and washed with excess of chloroform. The solvent from the filtrate was evaporated and the residue obtained was passed through a column of basic alumina using chloroform as an eluant. The material obtained on removal of chloroform was further purified by repeated crystallization using a mixture of chloroform and acetonitrile. Yield 0.28g (80%), m. p.142.0˚C. ν_{max}: 2922, 2852, 2667, 1745, 1739, 1737, 1712, 1461, 1377, 1280 cm^{-1}; δ_H: 8.54 (s, 2H, 2 × -CH═N-), 8.32 (d, ^3J 8.31 Hz, 4H, Ar-H), 8.10 (d, ^3J 8.52 Hz, 4H, Ar-H), 8.07 (d, ^3J 8.36 Hz, 4H, Ar-H), 7.53 (t, ^3J 8.18 Hz, 1H, Ar-H), 7.26 (d, ^3J 8.48 Hz, 4H, Ar-H), 7.25-7.21 (m, 3H, Ar-H), 4.33 (t, ^3J 6.64 Hz, 4H, 2 × Ar-COO-CH_2-), 1.82-1.75 (quin, ^3J 7.0 Hz, 4H, 2 × Ar-COO-CH_2-$\underline{CH_2}$-), 1.55-1.27 (m, 12H, 2 × (-CH_2-)$_3$), 0.88 (t, ^3J 6.8 Hz, 6H, 2 × -CH_3); $C_{48}H_{48}N_2O_8$ requires C 73.83, H 6.19, N 3.59; found C 74.25, H 5.98, N 3.39 %.

1, 3-Phenylene bis [4-(4-*n*-heptyloxycarbonylphenyliminomethyl)benzoate], 4.A.2

Yield 82%, m. p.140.5˚C. ν_{max}: 2952, 2922, 2852, 1745, 1737, 1712, 1569, 1456, 1434, 1411, 1278 cm^{-1}; δ_H: 8.54 (s, 2H, 2 × -CH═N-), 8.32 (d, ^3J 8.31 Hz, 4H, Ar-H), 8.10 (d, ^3J 8.52 Hz, 4H, Ar-H), 8.07 (d, ^3J 8.36 Hz, 4H, Ar-H), 7.53 (t, ^3J 8.18 Hz, 1H, Ar-H), 7.26 (d, ^3J 8.48 Hz, 4H, Ar-H), 7.25-7.21 (m, 3H, Ar-H), 4.33 (t, ^3J 6.64 Hz, 4H, 2 × Ar-COO-CH_2-), 1.82-1.75 (quin, ^3J 7.0 Hz, 4H, 2 × Ar-COO-CH_2-$\underline{CH_2}$-), 1.55-1.27 (m, 16H, 2 × (-CH_2-)$_4$), 0.88 (t, ^3J 6.8 Hz, 6H, 2 ×

-CH_3); $C_{50}H_{52}N_2O_8$ requires C 74.24, H 6.48, N 3.46; found C 74.41, H 6.39, N 3.18 %.

1, 3-Phenylene bis [4-(4-*n*-octyloxycarbonylphenyliminomethyl)benzoate], 4.A.3

Yield 85%, m. p.140.0˚C. ν_{max}: 3051, 2920, 2852, 1737, 1712, 1710, 1625, 1596, 1569, 1411, 1278, 1232, 1105, 1076 cm^{-1}; δ_H: 8.54 (s, 2H, 2 × -CH═N-), 8.32 (d, ^3J 8.31 Hz, 4H, Ar-H), 8.10 (d, ^3J 8.52 Hz, 4H, Ar-H), 8.07 (d, ^3J 8.36 Hz, 4H, Ar-H), 7.53 (t, ^3J 8.18 Hz, 1H, Ar-H), 7.26 (d, ^3J 8.48 Hz, 4H, Ar-H), 7.25-7.21 (m, 3H, Ar-H), 4.33 (t, ^3J 6.64 Hz, 4H, 2 × Ar-COO-CH_2-), 1.82-1.75 (quin, ^3J 7.0 Hz, 4H, 2 × Ar-COO-CH_2-$\underline{CH_2}$-), 1.55-1.27 (m, 20H, 2 × (-CH_2-)$_5$), 0.88 (t, ^3J 6.8 Hz, 6H, 2 × -CH_3); $C_{52}H_{56}N_2O_8$ requires C 74.60, H 6.70, N 3.34; found C 74.24, H 6.67, N 3.29 %.

1, 3-Phenylene bis [4-(4-*n*-nonyloxycarbonylphenyliminomethyl)benzoate], 4.A.4

Yield 83%, m. p.132.5˚C. ν_{max}: 3058, 2920, 2852, 1737, 1712, 1710, 1625, 1596, 1569, 1411, 1276, 1232, 1134, 1105, 1076 cm^{-1}; δ_H: 8.54 (s, 2H, 2 × -CH═N-), 8.32 (d, ^3J 8.31 Hz, 4H, Ar-H), 8.10 (d, ^3J 8.52 Hz, 4H, Ar-H), 8.07 (d, ^3J 8.36 Hz, 4H, Ar-H), 7.53 (t, ^3J 8.18 Hz, 1H, Ar-H), 7.26 (d, ^3J 8.48 Hz, 4H, Ar-H), 7.25-7.21 (m, 3H, Ar-H), 4.33 (t, ^3J 6.64 Hz, 4H, 2 × Ar-COO-CH_2-), 1.82-1.75 (quin, ^3J 7.0 Hz, 4H, 2 × Ar-COO-CH_2-$\underline{CH_2}$-), 1.55-1.27 (m, 24H, 2 × (-CH_2-)$_6$), 0.88 (t, ^3J 6.8 Hz, 6H, 2 × -CH_3); $C_{54}H_{60}N_2O_8$ requires C 74.98, H 6.99, N 3.24; found C 75.46, H 7.12, N 3.01 %.

1, 3-Phenylene bis [4-(4-*n*-decyloxycarbonylphenyliminomethyl)benzoate], 4.A.5

Yield 86%, m. p.134.5˚C. ν_{max}: 3058, 2918, 2850, 1737, 1712, 1710, 1625, 1596, 1569, 1411, 1276, 1232, 1134, 1105, 1076 cm^{-1}; δ_H: 8.54 (s, 2H, 2 × -CH═N-), 8.32 (d, ^3J 8.31 Hz, 4H, Ar-H), 8.10 (d, ^3J 8.52 Hz, 4H, Ar-H), 8.07 (d, ^3J 8.36 Hz, 4H, Ar-H), 7.53 (t, ^3J 8.18 Hz, 1H, Ar-H), 7.26 (d, ^3J 8.48 Hz, 4H, Ar-H), 7.25-7.21 (m, 3H, Ar-H), 4.33 (t, ^3J 6.64 Hz, 4H, 2 × Ar-COO-CH_2-), 1.82-1.75 (quin, ^3J 7.0 Hz, 4H, 2 × Ar-COO-CH_2-$\underline{CH_2}$-), 1.55-1.27 (m, 28H, 2 × (-CH_2-)$_7$), 0.88 (t, ^3J 6.8 Hz, 6H, 2 × -CH_3); $C_{56}H_{64}N_2O_8$ requires C 75.30, H 7.22, N 3.14; found C 74.96, H 7.07, N 3.15 %.

1, 3-Phenylene bis [4-(4-*n*-undecyloxycarbonylphenyliminomethyl)benzoate], 4.A.6

Yield 81%, m. p.132.5˚C. ν_{max}: 3051, 2920, 2850, 1737, 1712, 1710, 1625, 1596, 1569, 1411, 1276, 1232, 1134, 1105, 1076 cm^{-1}; δ_H: 8.54 (s, 2H, 2 × -CH═N-), 8.32 (d, ^3J 8.31 Hz, 4H, Ar-H), 8.10 (d, ^3J 8.52 Hz, 4H, Ar-H), 8.07 (d, ^3J 8.36 Hz, 4H, Ar-H), 7.53 (t, ^3J 8.18 Hz, 1H, Ar-H), 7.26 (d, ^3J 8.48 Hz, 4H, Ar-H), 7.25-7.21 (m, 3H, Ar-H), 4.33 (t, ^3J 6.64 Hz, 4H, 2 × Ar-COO-CH_2-), 1.82-1.75 (quin, ^3J 7.0 Hz, 4H, 2 × Ar-COO-CH_2-$\underline{CH_2}$-), 1.55-1.27 (m, 32H, 2 × $(-CH_2-)_8$), 0.88 (t, ^3J 6.8 Hz, 6H, 2 × -CH_3); $C_{58}H_{68}N_2O_8$ requires C 75.62, H 7.44, N 3.04; found C 75.97, H 7.47, N 2.74 %.

1, 3-Phenylene bis [4-(4-*n*-dodecyloxycarbonylphenyliminomethyl)benzoate], 4.A.7

Yield 87%, m. p.133.0˚C. ν_{max}: 3084, 2954, 2918, 2848, 1745, 1737, 1712, 1596, 1278, 1168 cm^{-1}; δ_H: 8.54 (s, 2H, 2 × -CH═N-), 8.32 (d, ^3J 8.31Hz, 4H, Ar-H), 8.10 (d, ^3J 8.52 Hz, 4H, Ar-H), 8.07 (d, ^3J 8.36 Hz, 4H, Ar-H), 7.53 (t, ^3J 8.18 Hz, 1H, Ar-H), 7.26 (*d*, ^3J 8.48 Hz, 4H, Ar-H), 7.24-7.21 (m, 3H, Ar-H), 4.33 (t, ^3J 6.64 Hz, 4H, 2 × Ar-COO-CH_2-), 1.82-1.75 (quin, ^3J 7.0 Hz, 4H, 2 × Ar-COO-CH_2-$\underline{CH_2}$-), 1.55-1.27 (m, 36H, 2 × $(-CH_2-)_9$), 0.88 (t, ^3J 6.8 Hz, 6H, 2 × -CH_3); $C_{60}H_{72}N_2O_8$ requires C 75.95, H 7.65, N 2.95; found C 76.4, H 7.76, N 2.64 %.

1, 3-Phenylene bis [4-(4-*n*-tridecyloxycarbonylphenyliminomethyl)benzoate], 4.A.8

Yield 80%, m. p. 131.0˚C. ν_{max}: 2952, 2920, 2848, 1745, 1739, 1737, 1712, 1596, 1467, 1278 cm^{-1}; δ_H: 8.54 (s, 2H, 2 × -CH═N-), 8.32 (d, ^3J 8.32 Hz, 4H, Ar-H), 8.11 (d, ^3J 8.52 Hz, 4H, Ar-H), 8.07 (d, ^3J 8.36 Hz, 4H, Ar-H), 7.53 (t, ^3J 8.18 Hz, 1H, Ar-H), 7.26 (d, ^3J 8.48 Hz, 4H, Ar-H), 7.24-7.21 (m, 3H, Ar-H), 4.33 (t, ^3J 6.64 Hz, 4H, 2× Ar-COO-CH_2-), 1.82-1.75 (quin, ^3J 6.76 Hz, 4H, 2 × Ar-COO-CH_2-$\underline{CH_2}$-), 1.55-1.26 (m, 40H, 2 × $(-CH_2-)_{10}$), 0.88 (t, ^3J 6.7 Hz, 6H, 2 × -CH_3); $C_{62}H_{76}N_2O_8$ requires C 76.20, H 7.83, N 2.87; found C 75.83, H 7.45, N 2.85 %.

1, 3-Phenylene bis [4-(4-*n*-tetradecyloxycarbonylphenyliminomethyl)benzoate], 4.A.9

Yield 83%, m. p.131.0˚C. ν_{max}: 2922, 2852, 1737, 1732, 1726, 1718, 1463,1280 cm^{-1}; δ_H: 8.54 (s, 2H, 2 × -CH═N-), 8.32 (d, ^3J 8.32 Hz, 4H, Ar-H), 8.11 (d, ^3J 8.48Hz, 4H, Ar-H), 8.07 (d, ^3J 8.32 Hz, 4H, Ar-H), 7.53 (t, ^3J 8.12 Hz, 1H, Ar-H), 7.26 (d, ^3J 8.48 Hz, 4H, Ar-H), 7.24-7.21 (m, 3H, Ar-H), 4.33 (t, ^3J 6.64 Hz, 4H, 2 × Ar-COO-CH_2-), 1.82-1.75 (quin, ^3J 7.0 Hz, 4H, 2 × Ar-COO-

CH_2-$\underline{CH_2}$-), 1.53-1.27 (m, 44H, 2 × (-CH_2-)$_{11}$), 0.87 (t, ^3J 6.8 Hz, 6H, 2 × -CH_3); $C_{64}H_{80}N_2O_8$ requires C 76.46, H 8.02, N 2.79; found C 75.98, H 7.91, N 2.45 %.

1, 3-Phenylene bis [4-(4-*n*-hexadecyloxycarbonylphenyliminomethyl)benzoate], 4.A.10

Yield 86%, m. p.130.5˚C. ν_{max}: 2952, 2916, 2848, 1741, 1737, 1732, 1716, 1598, 1471, 1276 cm^{-1}; δ_H : 8.54 (s, 2H, 2 × -CH═N-), 8.32 (d, ^3J 8.32 Hz, 4H, Ar-H), 8.11 (d, ^3J 8.48 Hz, 4H, Ar-H), 8.07 (d, ^3J 8.32 Hz, 4H, Ar-H), 7.53 (t, ^3J 8.12 Hz, 1H, Ar-H), 7.26 (d, ^3J 8.48 Hz, 4H, Ar-H), 7.24-7.21 (m, 3H, Ar-H), 4.33 (t, ^3J 6.64 Hz, 4H, 2 × Ar-COO-CH_2-), 1.82-1.75 (quin, ^3J 7.0 Hz, 4H, 2 × Ar-COO-CH_2-$\underline{CH_2}$-), 1.53-1.27 (m, 52H, 2 × (-CH_2-)$_{13}$), 0.87 (t, ^3J 6.8 Hz, 6H, 2 × -CH_3); $C_{68}H_{88}N_2O_8$ requires C 76.95, H 8.30, N 2.63; found C 77.28, H 8.12, N 2.48 %.

1, 3-Phenylene bis [4-(4-*n*-octadecyloxycarbonylphenyliminomethyl)benzoate], 4.A.11

Yield 85%, m. p. 131.0˚C. ν_{max}: 2954, 2918, 2848, 1741, 1716, 1714, 1712, 1625, 1596, 1467, 1276, 1232 cm^{-1}; δ_H: 8.54 (s, 2H, 2 × -CH═N-), 8.32 (d, ^3J 8.32 Hz, 4H, Ar-H), 8.11 (d, ^3J 8.48 Hz, 4H, Ar-H), 8.07 (d, ^3J 8.32 Hz, 4H, Ar-H), 7.53 (t, ^3J 8.12 Hz, 1H, Ar-H), 7.26 (d, ^3J 8.48 Hz, 4H, Ar-H), 7.24-7.21 (m, 3H, Ar-H), 4.33 (t, ^3J 6.64 Hz, 4H, 2 × Ar-COO-CH_2-), 1.82-1.75 (quin, ^3J 7.0 Hz, 4H, 2× Ar-COO-CH_2-$\underline{CH_2}$-), 1.53-1.27 (m, 60H, 2 × (-CH_2-)$_{15}$), 0.87 (t, ^3J 6.8 Hz, 6H, 2 × -CH_3); $C_{72}H_{96}N_2O_8$ requires C 77.38, H 8.66, N 2.50; found C 76.94, H 8.64, N 2.27 %.

1, 3-Phenylene bis [4-(4-*n*-decyloxycarbonylbenzylideneamino)benzoate], 4.B.1

4-(4-*n*-Decyloxycarbonylbenzylideneamino)benzoic acid, **4.h.1** (0.4g, 0.98 mmol) was reacted with 1,3-dihydroxybenzene, **4.v** (0.054g, 0.49 mmol) in dry dichloromethane (15 ml) in presence of DCC (0.22g, 1.1 mmol) and a catalytic amount of DMAP. The mixture was stirred at room temperature for 24 hours. The precipitated urea was filtered off and the solvent from the filtrate was evaporated. The residue was dissolved in chloroform and filtered through a column of basic alumina. The product thus obtained on removal of the solvent was further purified by repeated crystallization using a mixture of chloroform and acetonitrile. Yield 0.35g (80%), m. p. 139.5˚C. ν_{max}: 2922, 2852, 1730, 1720, 1714, 1712, 1596, 1568, 1413, 1274, 1234, 1132, 1072, 1109, 1012 cm^{-1}; δ_H: 8.52 (s, 2H, 2 × -CH═N-), 8.23 (d, ^3J 8.48 Hz, 4H, Ar-H), 8.17 (d, ^3J 8.30 Hz, 4H, Ar-H), 8.01 (d, ^3J 8.32 Hz, 4H, Ar-H), 7.50 (t, ^3J 8.28 Hz, 1H, Ar-H), 7.30 (d, ^3J 8.48 Hz, 4H, Ar-H),

7.22-7.17 (m, 3H, Ar-H), 4.35 (t, ^3J 6.68 Hz, 4H, 2 × Ar-COO-CH_2-), 1.83-1.76 (quin, ^3J 6.72 Hz, 4H, 2 × Ar-COO-CH_2-C$\underline{H}_2$-), 1.46-1.26 (m, 28H, 2 × (-CH_2-)$_7$), 0.87 (t, ^3J 6.56 Hz, 6H, 2 × -CH_3); $C_{56}H_{64}N_2O_8$ requires C 75.31, H 7.22, N 3.14 found C 74.93, H 7.27, N 3.07 %.

1, 3-Phenylene bis [4-(4-*n*-undecyloxycarbonylbenzylideneamino)benzoate], 4.B.2

Yield 82%, m. p. 137.5˚C. ν_{max}: 2922, 2852, 1730, 1720, 1714, 1712, 1596, 1568, 1413, 1274, 1234, 1132, 1072, 1109, 1012 cm^{-1}; δ_H: 8.52 (s, 2H, 2 × -CH═N-), 8.23 (d, ^3J 8.48 Hz, 4H, Ar-H), 8.17 (d, ^3J 8.30 Hz, 4H, Ar-H), 8.01 (d, ^3J 8.32 Hz, 4H, Ar-H), 7.50 (t, ^3J 8.28 Hz, 1H, Ar-H), 7.30 (d, ^3J 8.48 Hz, 4H, Ar-H), 7.22-7.17 (m, 3H, Ar-H), 4.35 (t, ^3J 6.68 Hz, 4H, 2 × Ar-COO-CH_2-), 1.83-1.76 (quin, ^3J 6.72 Hz, 4H, 2 × Ar-COO-CH_2-C$\underline{H}_2$-), 1.46-1.26 (m, 32H, 2 × (-CH_2-)$_8$), 0.87 (t, ^3J 6.56 Hz, 6H, 2 × -CH_3); $C_{58}H_{68}N_2O_8$ requires C 75.62, H 7.43, N 3.04; found C 75.13, H 7.57, N 3.16 %.

1, 3-Phenylene bis [4-(4-*n*-dodecyloxycarbonylbenzylideneamino)benzoate], 4.B.3

Yield 78%, m. p. 136.0˚C. ν_{max}: 2922, 2852, 1737, 1732, 1714, 1703, 1596, 1568, 1413, 1274, 1234, 1132, 1072, 1109, 1012 cm^{-1}; δ_H: 8.52 (s, 2H, 2 × -CH═N-), 8.23 (d, ^3J 8.48 Hz, 4H, Ar-H), 8.17 (d, ^3J 8.30 Hz, 4H, Ar-H), 8.01 (d, ^3J 8.32 Hz, 4H, Ar-H), 7.50 (t, ^3J 8.28 Hz, 1H, Ar-H), 7.30 (d, ^3J 8.48 Hz, 4H, Ar-H), 7.22-7.17 (m, 3H, Ar-H), 4.35 (t, ^3J 6.68 Hz, 4H, 2 × Ar-COO-CH_2-), 1.83-1.76 (quin, ^3J 6.72 Hz, 4H, 2 × Ar-COO-CH_2-C$\underline{H}_2$-), 1.46-1.26 (m, 36H, 2 × (-CH_2-)$_9$), 0.87 (t, ^3J 6.56 Hz, 6H, 2 × -CH_3); $C_{60}H_{72}N_2O_8$ requires C 75.93, H 7.64, N 2.95; found C 75.52, H 7.76, N 2.92 %.

1, 3-Phenylene bis [4-(4-*n*-tetradecyloxycarbonylbenzylideneamino)benzoate], 4.B.4

Yield 80%, m. p. 133.0˚C. ν_{max}: 2952, 2918, 2848, 1720, 1716, 1625, 1593, 1471, 1409, 1357, 1280, 1132, 1074 cm^{-1}; δ_H: 8.52 (s, 2H, 2 × -CH═N-), 8.23 (d, ^3J 8.48 Hz, 4H, Ar-H), 8.17 (d, ^3J 8.30 Hz, 4H, Ar-H), 8.01 (d, ^3J 8.32 Hz, 4H, Ar-H), 7.50 (t, ^3J 8.28 Hz, 1H, Ar-H), 7.30 (d, ^3J 8.48 Hz, 4H, Ar-H), 7.22-7.17 (m, 3H, Ar-H), 4.35 (t, ^3J 6.68 Hz, 4H, 2 × Ar-COO-CH_2-), 1.83-1.76 (quin, ^3J 6.72 Hz, 4H, 2 × Ar-COO-CH_2-C$\underline{H}_2$-), 1.46-1.26 (m, 44H, 2 × (-CH_2-)$_{11}$), 0.87 (t, ^3J 6.56 Hz, 6H, 2 × -CH_3); $C_{64}H_{80}N_2O_8$ requires C 76.46, H 8.02, N 2.79; found C 76.0, H 7.86, N 2.61 %.

1, 3-Phenylene bis [4-(4-*n*-hexadecyloxycarbonylbenzylideneamino)benzoate], 4.B.5

Yield 83%, m. p. 132.5˚C. ν_{max}: 2952, 2918, 2848, 1720, 1716, 1625, 1593, 1471, 1409, 1357, 1280, 1132, 1074 cm^{-1}; δ_H: 8.52 (s, 2H, 2 × -CH═N-), 8.23 (d, ^3J 8.48 Hz, 4H, Ar-H), 8.17 (d, ^3J 8.30 Hz, 4H, Ar-H), 8.01 (d, ^3J 8.32 Hz, 4H, Ar-H), 7.50 (t, ^3J 8.28 Hz, 1H, Ar-H), 7.30 (d, ^3J 8.48 Hz, 4H, Ar-H), 7.22-7.17 (m, 3H, Ar-H), 4.35 (t, ^3J 6.68 Hz, 4H, 2 × Ar-COO-CH_2-), 1.83-1.76 (quin, ^3J 6.72 Hz, 4H, 2 × Ar-COO-CH_2-C$\underline{H}_2$-), 1.46-1.26 (m, 52H, 2 × $(-CH_2-)_{13}$), 0.87 (t, ^3J 6.56 Hz, 6H, 2 × -CH_3); $C_{68}H_{88}N_2O_8$ requires C 76.94, H 8.36, N 2.65; found C 76.52, H 8.79, N 2.99 %.

1, 3-Phenylene bis [4-(4-*n*-octadecyloxycarbonylbenzylideneamino)benzoate], 4.B.6

Yield 85%, m. p. 130.5˚C. ν_{max}: 2952, 2916, 2848, 1724, 1720, 1718, 1716, 1625, 1593, 1471, 1409, 1357, 1280, 1132, 1074 cm^{-1}; δ_H: 8.52 (s, 2H, 2 × -CH═N-), 8.23 (d, ^3J 8.48 Hz, 4H, Ar-H), 8.17 (d, ^3J 8.30 Hz, 4H, Ar-H), 8.01 (d, ^3J 8.32 Hz, 4H, Ar-H), 7.50 (t, ^3J 8.28 Hz, 1H, Ar-H), 7.30 (d, ^3J 8.48 Hz, 4H, Ar-H), 7.22-7.17 (m, 3H, Ar-H), 4.35 (t, ^3J 6.68 Hz, 4H, 2 × Ar-COO-CH_2-), 1.83-1.76 (quin, ^3J 6.72 Hz, 4H, 2 × Ar-COO-CH_2-C$\underline{H}_2$-), 1.46-1.26 (m, 60H, 2 × $(-CH_2-)_{15}$), 0.87 (t, ^3J 6.56 Hz, 6H, 2 × -CH_3); $C_{72}H_{96}N_2O_8$ requires C 77.38, H 8.66, N 2.5 found C 76.95, H 8.61, N 2.19 %.

References

[1] P. G. de Gennes, *The Physics of Liquid Crystals*, Clarendon Press, Oxford, p277 (1975).

[2] H. R. Brand, P. E. Cladis and H. Pleiner, *Eur. Phys. J. B*, **6**, 347 (1998).

[3] A. Jákli, D. Krüerke, H. Sawade and G. Heppke, *Phys. Rev. Lett.*, **86**, 5715 (2001).

[4] S. Rauch, P. Bault, H. Sawade, G. Heppke, G. G. Nair and A. Jákli, *Phys. Rev. E*, **66**, 021706 (2002).

[5] A. Jákli, G. G. Nair, H. Sawade and G. Heppke, *Liq. Cryst.*, **30**, 265 (2003).

[6] A. Eremin, S. Diele, G. Pelzl, H. Nadasi and W. Weissflog, *Phys. Rev. E*, **67**, 021702 (2003).

[7] J. P. Bedel, J. C. Rouillon, J. P. Marcerou, H. T. Nguyen and M. F. Achard, *Phys. Rev. E*, **69**, 061702 (2004).

[8] G. Pelzl, S. Diele, A. Jakli, C. Lischka, I. Wirth and W. Weissflog, *Liq. Cryst.*, **26**, 135 (1999).

[9] R. Amaranatha Reddy and B. K. Sadashiva, *Liq. Cryst*., **29**, 1365 (2002).

[10] R. Amaranatha Reddy and B. K. Sadashiva, *Liq. Cryst*., **30**, 273 (2003).

[11] H. N. Shreenivasa Murthy and B. K. Sadashiva, *Liq. Cryst*., **30**, 1051 (2003).

[12] H. N. Shreenivasa Murthy and B. K. Sadashiva, *J. Mater. Chem*., **13**, 2863 (2003).

[13] (a) J. P. Bedel, J. C. Rouillon, J. P. Marcerou, M. Laguerre, H. T. Nguyen and M. F. Achard, *Liq. Cryst.*, **27**, 1411 (2000). (b) J. P. Bedel, J. C. Rouillon, J. P. Marcerou, M. Laguerre, H. T. Nguyen and M. F. Achard, *Liq. Cryst*., **28**, 1285 (2001). (c) J. P. Bedel, J. C. Rouillon, J. P. Marcerou, M. Laguerre, H. T. Nguyen and M. F. Achard, *J. Mater. Chem*., **12**, 2214 (2002).

[14] D. M. Walba, E. Körblova, R. Shao, J. E. Maclennan, D. R. Link, M. A. Glaser and N. A. Clark, *Science*, **288**, 2181 (2000).

[15] (a) G. Heppke, D. D. Parghi and H. Sawade, *Ferroelectrics*, **243**, 269 (2000). (b) G. Heppke, D. D. Parghi and H. Sawade, *Liq. Cryst*., **27**, 313 (2000).

[16] D. S. Shankar Rao, G. G. Nair, S. Krishna Prasad, S. Anita Nagamani and C. V. Yelamaggad, *Liq. Cryst*., **28**, 1239 (2001).

[17] D. A. Coleman, J. Fernsler, N. Chattham, M. Nakata, Y. Takanishi, E. Körblova, D. R. Link, R. -F. Shao, W. G. Jang, J. E. Maclennan, O. Mondainn-Monval, C. Boyer, W.

Weissflog, G. Pelzl, L. -C. Chien, J. Zasadzinski, J. Watanabe, D. M. Walba, H. Takezoe and N. A. Clark, *Science*, **301**, 1204 (2003).

[18] R. Amaranatha Reddy and C. Tschierske, *J. Mater. Chem.*, **16**, 907 (2006).

[19] D. R. Link, G. Natale, R. Shao, J. E. Maclennan, N. A. Clark, E. Körblova and D. M. Walba, *Science*, **278**, 1924 (1997).

[20] J. Svoboda, V. Novotna, V. Kozmik, M. Glogarova, W. Weissflog, S. Diele and G. Pelzl, *J, Mater. Chem.*, **13**, 2104 (2003).

[21] H. N. Shreenivasa Murthy, M. Bodyagin, S. Diele, U. Baumeister, G. Pelzl and W. Weissflog, *J. Mater. Chem.*, **16**, 1634 (2006).

[22] M. F. Achard, J. P. Bedel, J. P. Marcerou, H. T. Nguyen and J. C. Rouillon, *Eur. Phys. J. E*, **10**, 129 (2003).

[23] V. Novotna, M. Kaspar, V. Hamplova, M. Glogarova, L. Lejcek, J. Kroupa and D. Pociecha, *J. Mater. Chem.*, **16**, 2031 (2006).

[24] R. B. Meyer and R. A. Pelcovits, *Phys. Rev. E*, **65**, 061704 (2002).

[25] J. Ortega, M. R. de la Fuente, J. Etxebarria, C. L. Folcia, S. Diez, J. A. Gallastegui, N. Gimeno, M. B. Ros and M. A. Perez-Jubindo, *Phys. Rev. E*, **69**, 011703 (2004).

[26] R. Amaranatha Reddy, B. K. Sadashiva and V. A. Raghunathan, *Chem. Mater*., **16**, 4050 (2004).

[27] R. Amaranatha Reddy, V. A. Raghunathan and B. K. Sadashiva, *Chem. Mater*., **17**, 274 (2005).

[28] (a) W. Weissflog, M. W. Schroder, S. Diele and G. Pelzl, *Adv. Mater.*, **15**, 630 (2003). (b) J. Etxebarria, C. L. Folcia, J. Ortega and M. B. Ros, *Phys. Rev. E*, **67,** 042702 (2003). (c) A. Jakli, Y. M. Huang, K. Fodor-Csorba, A. Vajda, G. Galli, S. Diele and G. Pelzl, *Adv. Mater.*, **15**, 1606 (2003).

[29] C. Keith, R. Amaranatha Reddy, A. Hauser, U. Baumeister and C. Tschierske, *J. Am. Chem. Soc.*, **128**, 3051 (2006).

[30] J. Thisayukta, Y. Nakayama and J. Watanabe, *Liq. Cryst*., **27**, 1129 (2000).

[31] J. Thisayukta, Y. Nakayama, S. Kawauchi, H. Takezoe and J. Watanabe, *J. Am. Chem. Soc*., **122**, 7441 (2000).

[32] H. N. Shreenivasa Murthy and B. K. Sadashiva, *Liq. Cryst*., **29**, 1223 (2002).

[33] G. Dantlgraber, A. Eremin, S. Diele, A. Hauser, H. Kresse, G. Pelzl and C. Tschierske, *Angew. Chem. Int. Ed. Engl.*, **41**, 2408 (2002).

[34] G. Dantlgraber, S. Diele and C. Tschierske, *Chem. Commun*., 2768 (2002).

[35] R. Amaranatha Reddy and B. K. Sadashiva, *Liq. Cryst.*, **30**, 1031 (2003).

[36] A. Eremin, S. Diele, G. Pelzl and W. Weissflog, *Phys. Rev. E,* **67**, 020702 (2003).

[37] J. Ortega, C. L. Folcia, J. Etxebarria, N. Gimeno and M. B. Ros, *Phys. Rev. E,* **68**, 011707 (2003).

[38] M. W. Schröder, S. Diele, G. Pelzl, U. Dunemann, H. Kresse and W. Weissflog, *J. Mater. Chem*., **13**, 1877 (2003). (b) M. W. Schröder, G. Pelzl, U. Dunemann and W. Weissflog, *Liq. Cryst*., **31**, 633 (2004).

[39] C. Keith, R. Amaranatha Reddy, H. Hahn, H. Lang and C. Tschierske, *Chem. Commun.*, 1898 (2004).

[40] R. Amaranatha Reddy and B. K. Sadashiva, *J. Mater. Chem*., **14**, 1936 (2004).

[41] C. Keith, R. Amaranatha Reddy and C. Tschierske, *Chem. Commun.*, 871 (2005).

[42] L. E. Hough and N. A. Clark, *Phys. Rev. Lett.*, **95**, 107802 (2005).

[43] S. K. Lee, S. Heo, J. G. Lee, K. Kang, K. Kumazawa, K. Nishida, Y. Shimbo, Y. Takanishi, J. Watanabe, T. Doi, T. Takahashi and H. Takezoe, *J. Am. Chem. Soc.*, **127**, 11085 (2005).

[44] K. Nishida, M. Cepic, W. J. Kim, S. K. Lee, S. Heo, J. G. Lee, Y. Takanishi, K. Ishikawa, K. Kang, J. Watanabe and H. Takezoe, *Phys. Rev. E,* **74**, 021704 (2006).

[45] Y. Lansac, P. K. Maiti, N. A. Clark and M. A. Glaser, *Phys. Rev. E,* **67**, 011703 (2003).